3-10-2010

Investigating the Use of Frequency Selective Surfaces in High Power Microwave Applications

Steven M. Pugh

Using FSS in HPM Applications

THESIS

Steven Pugh, Captain, USAF

AFIT/GE/ENG/10-25

DEPARTMENT OF THE AIR FORCE
AIR UNIVERSITY

AIR FORCE INSTITUTE OF TECHNOLOGY

Wright-Patterson Air Force Base, Ohio

The views expressed in this thesis are those of the author and do not reflect the official policy or position of the United States Air Force, Department of Defense, or the United States Government.

AFIT/GE/ENG/10-25

Investigating the use of Frequency Selective Surfaces in High Power Microwave Applications

THESIS

Presented to the Faculty

Department of Electrical and Computer Engineering

Graduate School of Engineering and Management

Air Force Institute of Technology

Air University

Air Education and Training Command

In Partial Fulfillment of the Requirements for the

Degree of Master of Science in Electrical Engineering

Steven Pugh, B.S.E.E.

Captain, USAF

25 Mar 2010

AFIT/GE/ENG/10-25

Investigating the use of Frequency Selective Surfaces in High Power Microwave Applications

Steven Pugh, B.S.E.E.
Captain, USAF

Approved:

Michael Havrilla
Dr. Michael J. Havrilla (Chairman) — 17 Mar 2010 — date

Wm. F. Bailey
Dr. William F. Bailey (Member) — 17 Mar 2010 — date

Dr. Andrew J. Terzuoli (Member) — 17 Mar 2010 — date

Abstract

This thesis explores new territory with the theoretical investigation of the use of Frequency Selective Surfaces (FSS) in High Power Microwave (HPM) applications. Work was performed in a simulation environment where rectangular and ring-shaped FSS elements were evaluated. Incident electric field levels of $0.5MV/m$ were propagated toward the FSS in a plane wave that was perpendicular to the surface. Results show that the total electric field in the apertures of the FSS can reach more than $6MV/m$. This necessitates the use of high strength dielectric materials surrounding the FSS to reduce the risk of electrical breakdown. It is shown that a dielectric of only $2.5mm$ thick on each side of the FSS eliminates the risk of breakdown.

Acknowledgements

To the three people that mean the most to me: my grandma, wife and daughter. Without whom, I never would have known how to live. I appreciate it!

Steven Pugh

Table of Contents

Page

List of Figures

List of Tables

List of Symbols

List of Abbreviations

Investigating the use of Frequency Selective Surfaces in High Power Microwave Applications

I. High Power Microwaves in Todays Arsenal

In this chapter the discussion ensues about the reality of non-lethal weapons and how the Frequency Selective Surface can play a role.

1.1 Weaponry

Recent history has seen the development and rapid growth in military weaponry, both conventional and unconventional. Breaking down each of those categories more, we can define the line between lethal and nonlethal weapons within each category. Being a relatively new technology, nonlethal weapons are becoming better understood and introduced into the arsenal every day. Examples of the different types of weapons may be seen in Table 1.1. While these lethal weapon types have proven useful in a show of force for one military to dominate or defend against another, the ability to distinguish between an enemy military force and the local civilian population have made the use of conventional weapons a less desirable option. Also, the development of precision guidance along with satellite imagery and critical intelligence have narrowed the scope of detection dramatically. This precision and battlefield information help to reduce the collateral damage to surrounding population and infrastructure.

Table 1.1: This table is a quick reference to give an idea of different types of weapons available and the whether they are lethal or not.

WEAPON TYPE	LETHAL	NONLETHAL
Conventional	Revolvers, Machine Gun, Assault Rifles, Mortars, Artillery, etc.	Tear Gas, Plastic Bullets, Tasers, Sprays, Water Cannon, etc.
Unconventional	Biological Toxins, Chemical Agents, etc.	High Power Microwaves, Low Energy Lasers, Acoustic Weapons, etc.

Nonlethal weapons are another option of weaponry that allows one force to prevent and possibly stop aggressive opponents, whether military or other. This happens with the knowledge that the nonlethal options not only reduce the collateral damage, but usually have reversible consequences. The use of nonlethal weapons provides an increasing array of capability that a commander may use to aid their troops in special situations where conventional lethal weapons would be too much to consider. Particularly, the nonlethal weapons pursued today, such as bean bag rounds, pepper sprays, spike strips and directed energy systems allow the warfighter to detect and deter potentially dangerous individuals, deny or stop suspicious vehicles, and disrupt electronic and optical systems. Like lethal weapons, nonlethal weapons have the ability to employ with safe standoff distance between the operators and the target of interest [5]. For this thesis, the scope of the nonlethal weapons will be focused on the use of High Power Microwave (HPM) weapon systems.

Referring to the guidelines from [2], High Power Microwave is defined as "coherent electromagnetic radiation spanning the frequency range of approximately 1 GHz to

Table 1.2: Possible applications for nonlethal weapons to be used in both the civilian and military communities.

Civilian (Law enforcement) Scenarios	**Military Scenarios**
Automobile chase	Unarmed crowd blocking a convoy
Illegal border crossing	Armed civilians blocking a convoy
Snipers shooting at civilians	Peace-enforcement and support efforts
Certain hostage situations	Suicide attack against military facilities
Suicide attack against public places	Large number of unarmed civilians hiding armed individuals
Riverboats carrying contraband	Area denial and perimeter security
Trucks carrying contraband	Enforcement of no-fly zones by attacking air defence facilities
	Violations of demilitarized zones (ex: tunneling through the DMZ in Korea)
	Deny successful mission to hostile aircraft and incoming missiles

over 100 GHz." HPM can then be broken down into two areas as high-average-power microwaves, which denotes that the pulse duration of the electromagnetic radiation will be longer duration and with high repetition or continuous beam. The alternative is the high-peak-power microwaves that implies sourced radiation with short pulse duration, a low repetition rate, also known as single shot source. All HPM sources are characterized by the amplitude of their source power. While these values range anywhere from $1KW$-$10GW$ and more, the problem at hand is going to consider the irradiance, or power delivered per unit area (W/m^2). Irradiance is associated with the time-average Poynting vector as

$$\mathbf{S} = \frac{1}{2}\mathrm{Re}[\mathbf{E} \times \mathbf{H}^*]. \tag{1.1}$$

These values will be quite high as to produce electric field levels near the breakdown of air upon exiting the system. Exploring the ways to handle the incident wave with such levels will become quite important in the design and implementation of frequency selective surfaces.

1.2 HPM/FSS combination

The goal of this research is to investigate the use of frequency selective surfaces (FSS) in HPM applications. The FSS would potentially be used as a radome on the director for the system. This would ideally reduce any out-of-band radar cross section (RCS) that would be seen reflecting from the HPM system. The challenge,

however, lies in the ability to efficiently transmit high energy signals through very small apertures in the FSS without risk of electromagnetic breakdown, or overheating the FSS that may cause damage. Particularly, the research presented will investigate the high electric fields that will become evident at the surface of the FSS.

To try and get a better idea on the subject matter, several steps will be pursued. As this is a relatively new research area, possible methods for work will be discussed, as well as, investigation into proposed methods for dealing with high power in FSS. The paper here is broken down in the following manner:

- Chapter 1: Introduce the general topic and concerns
- Chapter 2: Investigate available and possible methods for the research with supporting science
- Chapter 3: Go into detail about how the research will be performed
- Chapter 4: Discuss the results of the research
- Chapter 5: Explain briefly what the results revealed and potential future directions

II. Selecting Appropriate Frequency Selective Surface

This chapter investigates the research documents that were used in this work. Due to limited resources directly related to the current topic, some parallels were made with similar work.

2.1 Frequency Selective Surfaces

Frequency Selective Surfaces (FSS) are periodic structures with either patch or aperture elements placed in a two-dimensional periodic grid that have frequency filtering properties. These filtering properties are not unlike radio frequency (RF) circuits, where the FSS will transmit a low-pass or high-pass spectral signal due to its element type (patch or aperture).

Based on the work in [6], we find applications of FSS structures range from single to multiple frequency band-pass or band-stop uses. The need for such surfaces began to be studied shortly after radar applications were proving useful during World War II. Both allies and enemies were busy figuring out how to obtain, classify and use returns from radar that provided what we know as radar cross sections (RCS). Efforts were made on reducing the RCS of vehicles to disguise them from enemy radar. Radar absorbing materials were initially used to attempt to reduce the RCS with success. However, the antennas on aircraft proved to be the hardest areas to reduce. Since the user usually only needs a small frequency range of operation and the enemy could use the reflection of the antenna in many different frequencies, a solution was pursued. Investigations uncovered that using arrays of highly conducting elements

could at least limit the range of frequencies to penetrate the surface. This in turn led to more experiments to further optimize the use of such technology, including the realization of either transmitting or reflecting particular frequencies. FSS uses can present both mechanical and electromagnetic protection to antennas [10]. FSS are also used as dichroic plates in reflector systems, bandpass radomes, bandstop filters, circuit analog absorbers, etcetera [6].

An FSS made up of patches, as in 2.1b, consists of arbitrarily shaped conducting material that supports electric currents. The complement of the patch FSS is one made up of arbitrarily shaped apertures cut out of a metallic sheet, essentially a screen, as depicted in figure 2.1a. The aperture FSS will support equivalent *magnetic* currents within the apertures. In the study of electromagnetics, one can use so called *magnetic* current to describe the way fields propagate from a slot into free space. The math turns out to be exactly the same form as when describing the propagation of fields from a dipole or other conducting surface with an alternating current applied.

Several design parameters become vitally important to the success of the periodic surfaces. The particular element size, shape and thickness, as well as their periodic spacing, surrounding media and any additional FSS grids stacked onto one another influence the transmission and reflection characteristics of the FSS. Each FSS must be designed and tested independently for each application needed. The dimensions, when chosen properly, may exhibit characteristics that pass, or reflect, electromagnetic (EM) waves at a particular frequency.

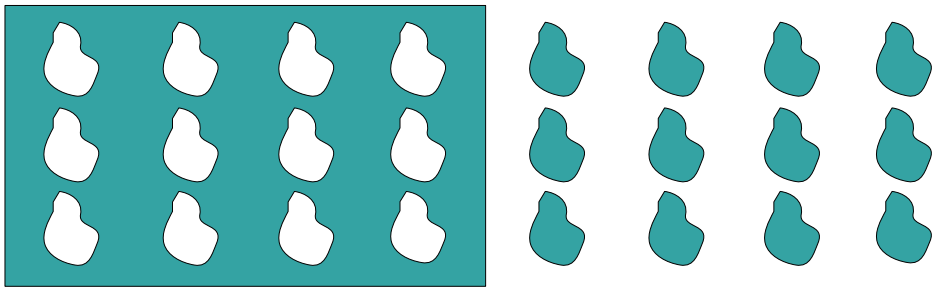

(a) Aperture FSS

(b) Patch FSS

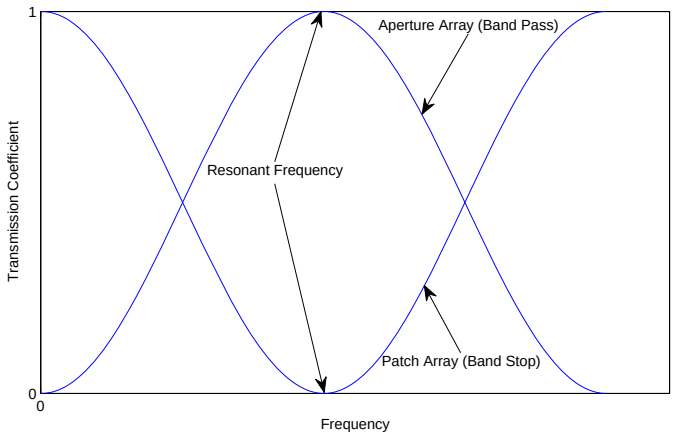

(c) Frequency Response

Figure 2.1: Arbitrary shaped FSS that depicts the complementary nature of the two different methods. The patches generally will reflect a certain frequency band, while the aperture type of FSS will transmit a certain frequency band. The frequency response is shaped according to size, shape, orientation to incident field, and even number of surfaces stacked together.

In the high power microwave (HPM) application of this research, we need to provide the most efficient method of transmission possible. Another way of looking at it is to have as little reflection as possible. A big challenge using HPM systems is the ability to get the high power signal from the antenna to the intended target with little degradation. Therefore all inhibitors need to be eliminated or minimized for maximum system performance.

Examples of HPM use with FSS is minimal. However, similar work has been investigated in [3], which investigates the performance of an FSS with rectangular-shaped elements. The authors, Chen and Stanton of California Institute of Technology, were studying ways of providing a structurally sound FSS for space-based applications. The structurally sound part implies that the grid be of a thick metal, therefore presenting a sort of lattice of small waveguides.

The basic premise of an FSS is that the elements will resonate at the given frequency. One example would involve the vibrations of a string fixed between two points. When the string is plucked, it will oscillate back and forth in the shape of a wave, while the ends will be held at the fixed locations. This oscillation is essentially the resonant frequency of that string. Antennas work similarly and will be discussed in the next section.

2.2 Antenna Theory Similarity

It's appropriate to look at the far zone electromagnetic (EM) fields radiated by an antenna. This will give a somewhat better view of how the field interacts

with another antenna in free space, as well as provide information as to how to design the antenna, or in our case the FSS, to gain optimal performance. The far zone electromagnetic field derived from Maxwell's equations that is radiated from an arbitrary antenna may be expressed as

$$\vec{E}(r,\theta,\phi) = [\hat{\theta}F_\theta(\theta,\phi) + \hat{\phi}F_\phi(\theta,\phi)]\frac{e^{-jk_0r}}{r}\text{V/m}, \tag{2.1}$$

where $\vec{E}$ is the electric field vector in spherical coordinates that has $\hat{\theta}$ and $\hat{\phi}$ vector components. The free space propagation constant is $k_0 = 2\pi/\lambda$, with wavelength $\lambda = c/f$. This equation assumes that there is a negligible radial component ($\hat{r}$) in the electromagnetic wave, which will also play a role in the design of an FSS element geometry to take advantage of the polarization of the wave. The radial distance r from the radiating source does affect the phase variation as e^{-jk_0r} and the amplitude variation as $1/r$.

An incident sinusoidal wave interacts with the antenna and induces an electric current. If the antenna length is a multiple of a half-wavelength, then

$$2d = n\lambda, \qquad n \in \{1, 2, 3 \ldots\}, \tag{2.2}$$

where d is the length of the antenna and λ is the wavelength of the wave. If the design frequency (f) is known and a wave is traveling at velocity v, then λ is given by

$$\lambda = v/f. \tag{2.3}$$

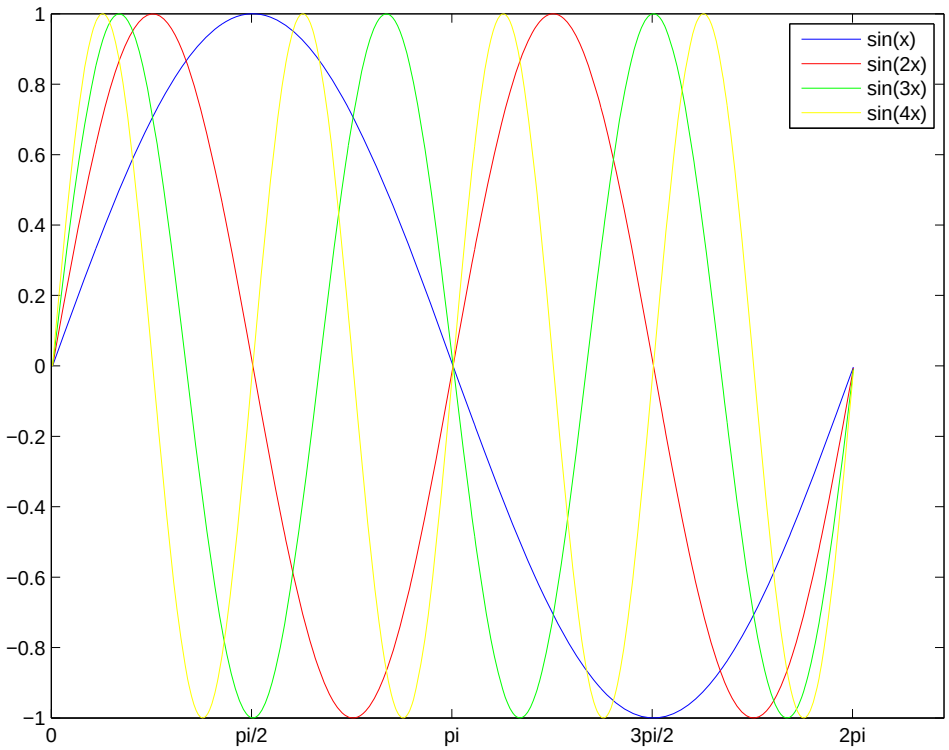

Figure 2.2: Sine wave showing first four harmonics.

Antennas that are multiples of one wavelength long will, in turn, fit a corresponding number of periods of the incident wave on the antenna at one time and will resonate. Figure 2.2 displays the simple visualization of the sine wave with the first four harmonics.

In the case of FSS, the EM wave with a matching wavelength to the element length will pass through the element (or reflect in case of the patch FSS), while any other wavelength will be reflected. The cutoff will roll off and not be abrupt, however encasing the FSS in dielectric will increase the cutoff slope. Also, placing the elements closer together will reduce the chance of grating lobes being introduced [6].

Particularly, the elements need to be closer than $\lambda/2$ wavelengths to suppress the grating lobes. This is another fact based on array antenna theory.

2.3 FSS Element geometry

The element shape is important in the design of the FSS in that it will affect the efficiency to handle oblique incident EM waves, cross-polarization, bandwidth and band separation. An easy shape to analyze is the rectangular dipole. It has good transmission properties with vertically polarized waves and good frequency band separation. A drawback of the rectangular dipole is the inability to transmit waves with oblique angles effectively. Essentially, the dipole will resonate with incident wave, but the transmitted frequency shifts [11].

The dipole elements will resonate if their length is a multiple of a half-wavelength. As the length goes up in multiples of one half, the number of nulls in the radiated pattern will go up as well. For instance, a one wavelength length will have one null and 1.5 wavelength length will have two nulls [11].

The dipole elements, or basic rectangular shape, have some drawbacks concerned with the ability to resonate if the incident angle of the EM fields are such that they don't line up correctly with the elements. If the incident field is rotated with respect to the elements as in Figure 2.3, then part, up to all, of the energy will be reflected. Therefore, using dipole-shaped elements in a radome application where the radome is not planar, or the incidence of angles are not fixed, is not advantageous.

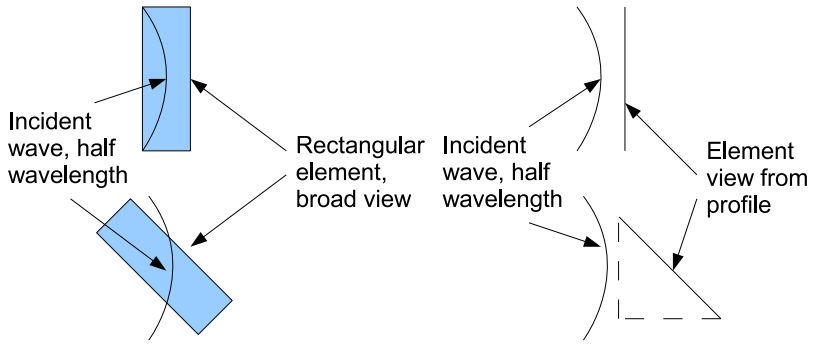

(a) Broad view of Surface (b) Profile view of Surface

Figure 2.3: Rectangular elements the size $\lambda/2$ of an incident field wavelength as seen. Figure 2.3a on top shows correct alignment with the half wavelength fitting the length of the element, while the bottom picture is of the field is incident on a rotated angle. Likewise, figure 2.3b shows an incident angle from the broadside of the surface. Both depict that with various angles of incidence, the alignment would potentially, adversely affect the transmission/reflection characteristics of the surface.

A ring shape is more appropriate for the curved FSS application, or one where the incident wave will form an oblique angle to the surface. The ring elements have an advantage over others shapes such as rectangular dipoles in that they are invariant to any polarization of the incident EM wave and they are not sensitive to the angle of incident [10].

Loop elements, square or round, will resonate when the length of half the loop is a multiple of a half-wavelength. Basically each half loop acts as one dipole element and has similar properties as noted above. Therefore, the circumference should be the length of one wavelength to avoid nulls in the scattered pattern.

A widely cited article by Parker and Hamdy to *Electronics Letters* [7] gives many reasons for using ring shaped elements in frequency selective surfaces. In their letter, Parker and Hamdy look at conducting rings placed closely together in a periodic

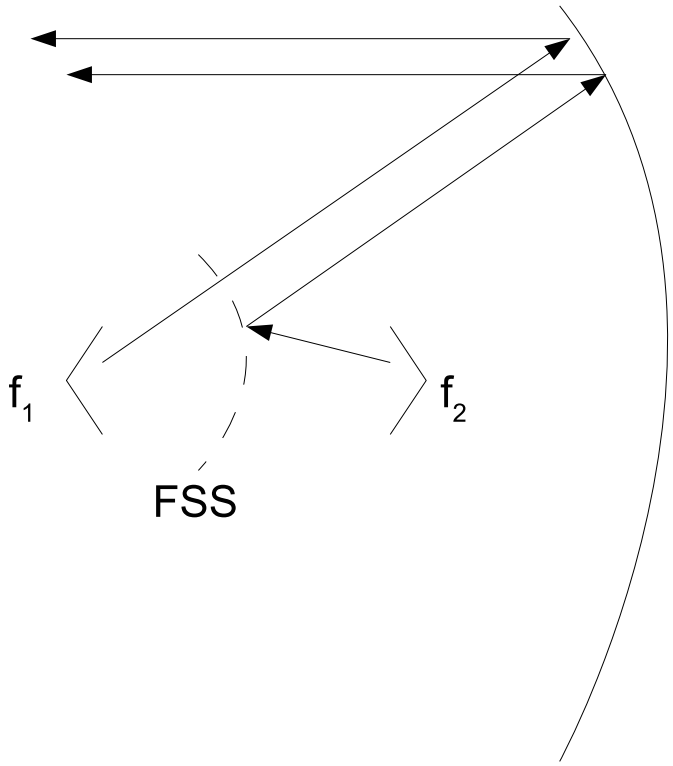

Figure 2.4: Dichroic subreflector system drawing replicated from one in [6] that shows the orientation of the FSS in relation to two different frequency feeds. The FSS has the responsibility to pass the frequency from f_1, while reflecting the frequency from the feed f_2.

array. The main objective of their study was an application to be used in reflector antennas.

Reflector antennas, as depicted in Figure 2.4, are used in systems that require two different frequencies for operation, therefore a need to direct one frequency to a particular transmitter/receiver while at the same time allowing energy from another frequency to pass to a second transmitter/receiver is desired. The premise uses the true nature of frequency selective surfaces to be transparent at one frequency and reflective at another frequency, hence utilizing the different placement and orientation of the feed horn.

With their motivation, Parker and Hamdy set up an experiment with a closely spaced, equilateral triangular lattice as in Figure 2.5. The rings had a radius of $2.0mm$ at the center of the conductor and thickness of $0.4mm$, with a separation D of $4.9mm$ from center to center of the rings. Then the array was printed on a $20cm$ diameter circle of a dielectric substrate with a relative permittivity $\epsilon_r = 2.33$. They illuminated the sample with a plane wave and varied the angle of incidence from $0^\circ - 45^\circ$. The range of variation of the angles of incidence is representative of what the dichroic subreflector would experience.

Their experiments revealed that varying angles of incidence from $0^\circ - 45^\circ$ did not affect the transmission characteristics of the surface in either the E-plane or the H-plane.

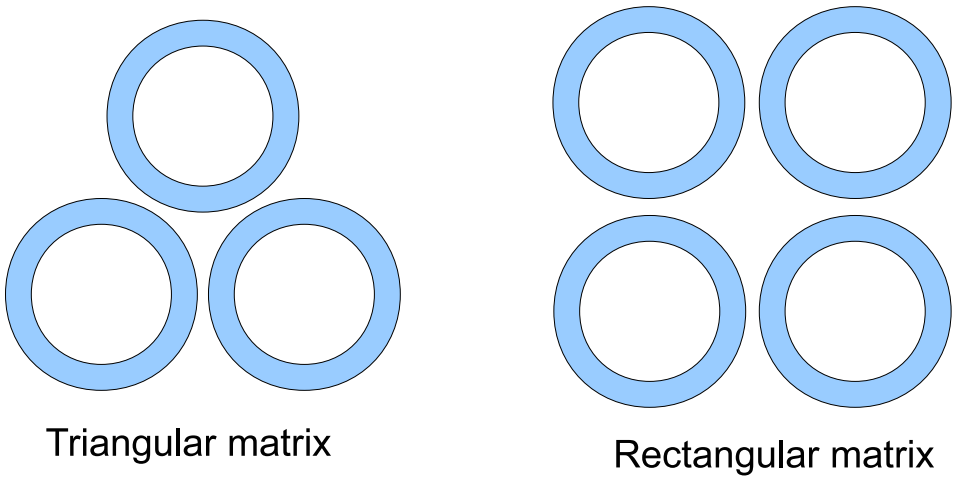

Figure 2.5: Ring layout as used in the experiments in [7] where the triangular grid provides the ability to bring the elements closer together than that of the rectangular grid. Parker and Hamdy were able to prove that the closer spaced triangular grid performs better than the rectangular grid when the angle of incidence increases. They showed that the frequency reflection curves hardly shifted in either the E-plane or the H-plane in the triangular case, but both the E-plane and the H-plane curves shifted when using the rectangular lattice.

To vary the experiment, Parker and Hamdy used a square lattice with relative measurements $2r/D = 0.62$ instead of the triangular dimensions that gave the previous $2r/D = 0.82$. With wider spacing, they revealed a devrease from $35.6GHz$ to about $32.1GHz$ in the H-plane when the angle of incidence increased from $0°$ to $45°$. The E-plane also experienced a drop of about $2GHz$.

The work they performed proved that using ring elements that are closely spaced is a good choice for the dichroic subreflectors because of the consistency of frequency response when compared to angle of incidence as it varied from $0°$ to $45°$. Thier research also revealed that about 26 percent reflection bandwidth was measured where reflection coefficient fell below $-0.5dB$ for the range of angles.

2.4 Breakdown issues

Chen performed an analysis on the thick FSS that shows the characteristics associated with scattering of such an object. This approach was needed for a space application of the paper, however the thickness will prove to be required for heat transfer of high power applications as well [3]. Since FSS may be either arrays of metallic elements, or by the complementary principle, arrays of slots, the application will determine the necessary geometry. Also, each has its own transmission characteristics that perform in different aspects. Since this research will be dealing with high-power (greater than 0.5 megawatts), the ability to dissipate heat will need to be addressed. If small, thin metallic elements are used, the risk of heating the metal to melting point is a critical concern. Thus, to reduce this risk, the slot FSS is chosen for analysis in this thesis effort.

Other ways to reduce the heat is to pick low loss dielectrics that sandwich the conducting surface. Loss in a material is due to friction which is caused by the movement of electrons within the material. This friction will create heat and due to conservation of energy will be converted from the incident wave's energy. Therefore, with low loss materials, they will not heat up as much or as fast. Another factor is to select materials that have similar coefficients of thermal expansion so they will not contract and expand at such different rates to create gaps between the two materials. With that, picking materials that have high thermal conductivity is key to helping divert heat away from the areas of high energy acting like a built-in heat sink. Lastly,

one should consider the manner in which to dissipate the heat generated from the FSS. This may be done by connecting to an actual heat sink [4].

Once thermal breakdown has been considered, voltage breakdown will need to be addressed. This may happen in the slots due to the electric field becoming greater than the breakdown limit of the air or dielectric in the slots during peak power. The electric field in the slot comes from a build up of the positive and negative charges applied to the edges of the slot top and bottom. They are evanescent fields that act as reactive or stored energy. These evanescent fields need to be added to the incident fields to get a total field in the location right at the slot. Once the total field has been calculated, one would be able to determine whether a breakdown will occur within the aperture [4].

III. Simulation Assumptions and Settings

The assumptions and settings for the FSS simulations are discussed in this chapter.

3.1 Choosing correct attributes

To start experimenting with the potential use of Frequency Selective Surfaces (FSS) in High Power Microwave (HPM) applications, one must examine the specific application and design the FSS that would be appropriate for the situation. In particular, the FSS has to be able to transmit as much energy as possible in the desired direction. At the same time, the heat dissipation must be effective. Since we will be investigating band pass surfaces, the best element type to use is slots. Thus, using that information the metal barrier will provide sufficient area for heat dissipation. Not only the metal will be taken into consideration, but also the dielectric material surrounding the metal surface must be an integral part of the design [6]. The two materials need to be chosen to have very similar heat diffusion properties so they can work in tandem. This quality will also insure that the two materials do not expand and contract at different rates as to introduce air gaps. The air gaps may be just enough to allow an electromagnetic breakdown and produce an arc across the apertures. Such an occurrence would be detrimental to system performance as the arc essentially induces a short-circuit across the aperture, thus reflecting the incident waves.

The shape of the slot will be chosen to be able to work with the geometry of the application. In other words, the qualities of the signal (incoming, outgoing,

polarization, angle of incidence, etc.) need to be considered. The polarization is easily accommodated with shapes that will resonate with any combination of signal (linear, circular, or elliptical). These will have two dimensions such as a three legged element, Jerusalem cross, or as simple as a ring. Some shapes have better transmission characteristics at angles of incidence other than perpendicular. For instance the ring element has been shown to exhibit just this behavior (ref the ring element papers). For radome-type application, where limiting the out-of-band radar cross section of the antenna is important, such shapes that transmit effectively at oblique angles would need to be considered as will be seen in the development of this chapter.

3.2 Confirming the element shape

To check the ability to transmit and reflect signals, the FSS was simulated in the software CST MICROWAVE STUDIO®. The actual utility that was used is the frequency domain solver. Within this solver, the simulation iteratively stepped through a specified frequency range and provide results on a two dimensional S-parameter plot.

In [11], the reader is given an overview on how scattering parameters (S-parameters) are defined. Figure 3.1 displays the incident and reflected fields as incoming and outgoing waves, (a_1, a_2) and (b_1, b_2), respectively. These incoming and outgoing waves are represented by complex amplitudes in terms of their voltage and

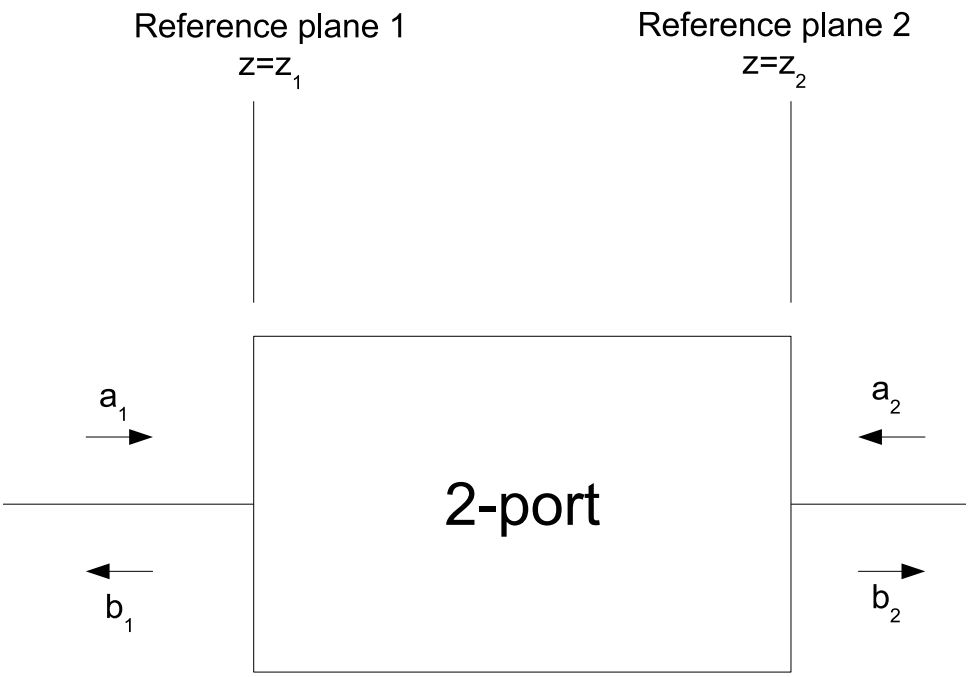

Figure 3.1: Two-port microwave circuit or network drafted from the text [11]. This is used as a guide to help understand the concept of scattering parameters.

currents at their reference planes. The representations are in the form

$$a_{(1,2)} = \frac{V(z_{(1,2)}, t)}{2\sqrt{Z_0}} + Z_0 \frac{I(z_{(1,2)}, t)}{2\sqrt{Z_0}}, \tag{3.1}$$

$$b_{(1,2)} = \frac{V(z_{(1,2)}, t)}{2\sqrt{Z_0}} - Z_0 \frac{I(z_{(1,2)}, t)}{2\sqrt{Z_0}}, \tag{3.2}$$

where Wu defines $z_{(1,2)}$ as the reference planes as seen in Figure 3.1 and t is the time, Z_0 is the characteristic impedance of the network, V is the voltage evaluated at z, and I is the current evaluated at z. The variables a and b have the units of $\sqrt{power}$

where the powers that are entering and leaving the network are represented by

$$P^{in} = \frac{1}{2}\left[a_1 a_1^* + a_2 a_2^*\right], \tag{3.3}$$

$$P^{out} = \frac{1}{2}\left[b_1 b_1^* + b_2 b_2^*\right]. \tag{3.4}$$

If the system is linear, then the input and output variables $a_{(1,2)}$ and $b_{(1,2)}$ are related by the introduction of the scattering parameters (S-parameters) as

$$b_1 = a_1 S_{11} + a_2 S_{12}, \tag{3.5}$$

$$b_2 = a_1 S_{21} + a_2 S_{22}. \tag{3.6}$$

The equations can then be put into matrix form as $\mathbf{b} = \mathrm{S}\mathbf{a}$, where

$$\mathbf{a} = \begin{bmatrix} a_1 \\ \\ a_2 \end{bmatrix}, \mathbf{b} = \begin{bmatrix} b_1 \\ \\ b_2 \end{bmatrix}, S = \begin{bmatrix} S_{11} & S_{12} \\ \\ S_{21} & S_{22} \end{bmatrix} \tag{3.7}$$

Then for evaluation purposes, especially in the case of the FSS, one of the incoming wave amplitudes may be set to zero. For instance, setting the right side incoming wave to zero (no source emitting a wave from that direction) will make $a_2 = 0$ which reveals

$$S_{11} = \frac{b_1}{a_1} \text{ and } S_{21} = \frac{b_2}{a_1}. \tag{3.8}$$

Note, this form can now be generalized to a n-port case where the the matrices can be expanded to a $n \times n$ for the scattering matrix and each of the vectors $\mathbf{a}$ and $\mathbf{b}$ will have n elements.

These S-parameters are also useful in evaluating the incident and scattered electromagnetic fields and how they interact with the FSS. This is going to be of interest to help determine whether or not an FSS transmits or reflects at the desired frequency or frequency band.

3.3 Concerning dielectrics

Other than the heat dissipation concern, the extreme electric fields need to be considered. These will vary based again on the shape of the elements and the orientation of the incident electric field. Consider a rectangular slot element as in Figure 3.2. The width of the gap in the rectangle will typically be wider than the width of the gap in a ring shaped element. This difference in the size of the aperture plainly shows that the electric field across the gap will vary considerably. The potential that is laid on either side of the opening will determine the electric field across the opening and that will come into play as the gap narrows. Since field strength increases as gap size decreases, breakdown becomes more likely.

A view of a rectangular element in an FSS shows how the impressed current density $\vec{J}_i$ on the surface will tend to flow in a path around the aperture openings. In the Figure 3.3, one can see that the same current will not flow through the apertures as noted before. So, charges build up and create a density on the edge of the aperture

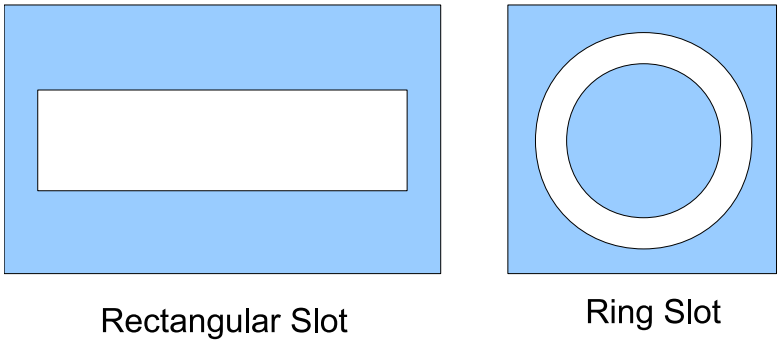

Figure 3.2: Example of two basic element shapes where the dimension of the slots may differ greatly. The rectangle can be quite large compared to the ring, while the ring has better transmission qualities for increased angles of incidence.

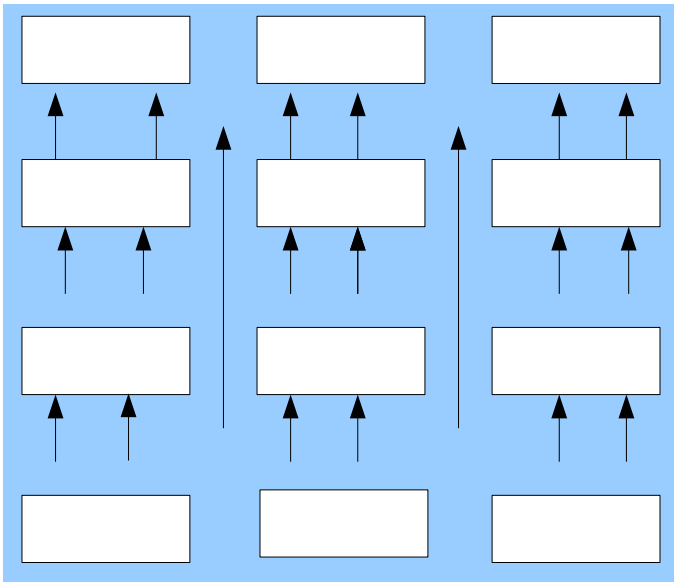

Figure 3.3: Induced current density $\vec{J}_i$ that is flowing on the surface of the FSS. The current represented by the arrows will naturally follow the path of least resistance, but will build up a net charge on either side of the elements where the surface ends, which in turn will create an electric field across the void.

as seen in Figure 3.4. From [1], the normal electric flux density ($\widehat{n} \cdot \vec{D}$) is equal to the free surface charge q_{es} due to the PEC. If a dielectric is added in the opening, then that equation takes the form

$$\widehat{n} \cdot (\epsilon_0 \vec{E} + \vec{P}) = q_{es}. \tag{3.9}$$

This equation introduces the polarization vector $\vec{P}$ such that

$$\epsilon_0 \widehat{n} \cdot \vec{E} + \widehat{n} \cdot \vec{P} = q_{es}, \tag{3.10}$$

where

$$\widehat{n} \cdot \vec{P} = q_{ps}, \tag{3.11}$$

and q_{ps} is the bound polarization surface charge due to the dielectric. Therefore the equation could be written as

$$\widehat{n} \cdot \vec{E} = \frac{q_{es} - q_{ps}}{\epsilon_0}, \tag{3.12}$$

which basically means that the more higher the bound surface charge due to the presence of the dielectric, the lower the normal electric field. This property will work to the advantage by reducing the electric field within the dielectric, which will also have a higher breakdown limit than that of air. This will lead to the need to find a dielectric with a desirable dielectric constant, or relative permittivity (ϵ_r).

The dielectric constant is a descriptive value for the dielectric material's ability to store charge (energy) relative to free space. Larger dielectric constants indicate

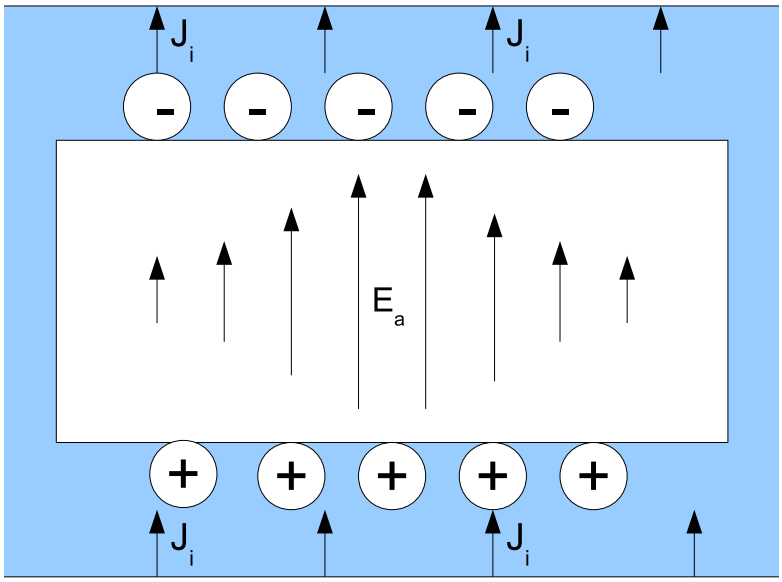

Figure 3.4: E-field created by the current impressed on the surface of the FSS. This is similar to the charges on the plates of a capacitor where an electric field is applied by the potential on the plates.

that the material is capable of storing more charge (energy). The energy storage attributes of dielectrics will be a factor when choosing one to implement in the high power application of FSS. We need the energy to pass through the FSS to avoid higher-order mode dispersion. Therefore a dielectric with low relative permittivity would be best. However, as in [6], the dielectric profile needs to be factored into the equation. Munk presents that using Fresnel transmission coefficients, thickness of dielectric $\lambda_e/4$ on each side of the slot FSS and a dielectric constant of around 1.5, a scan independence will appear for scan angles up to 60°. In other words the resonant frequency will remain stable for up to a 60° incident wave, but above that shift start to shift. Also if the dielectric constant increases or the thickness of the dielectric decreases, the independence will be smaller.

Dielectric strength will be as important in the HPM applications as their consistency in transmitting the signal. In [9] and [8], the authors studied the breakdown of a dielectric insulator that provided results in ranges well above the breakdown of air. While these were not really the same application, they do present hope that the dielectrics will hold up under extreme magnitudes of the applied electric fields without failing.

3.4 Picking the element shape

Experimenting with different element geometries gives an idea of the location of the peak electric field represented in each geometry. In rectangular elements, with normal incidence, the electric field is highest near the centers of the horizontal length. This is expected as the discontinuities between the conducting surface and the dielectric material are presented and tangential $\vec{E}$ must be zero at the left and right walls. Basically, the impressed currents on the metallic surface tend to want to travel in the least resistance path, for example around the aperture elements. However, right at the center these currents inevitably encounter the discontinuous nature of the surface. The electrons will then build at that surface, thus an electric field will develop in the aperture opening. The electric field will be greatest in the center due to the boundary conditions on the right and left edges of the aperture as seen in Figure 3.4. Balanis explains in [1] that when a medium contains infinite conductivity, the tangential electric fields will be equal to zero. Referring to Figure 3.5, the medium 1 will be assumed to have infinite conductivity ($\sigma_1 = \infty$). Therefore an electric field cannot be

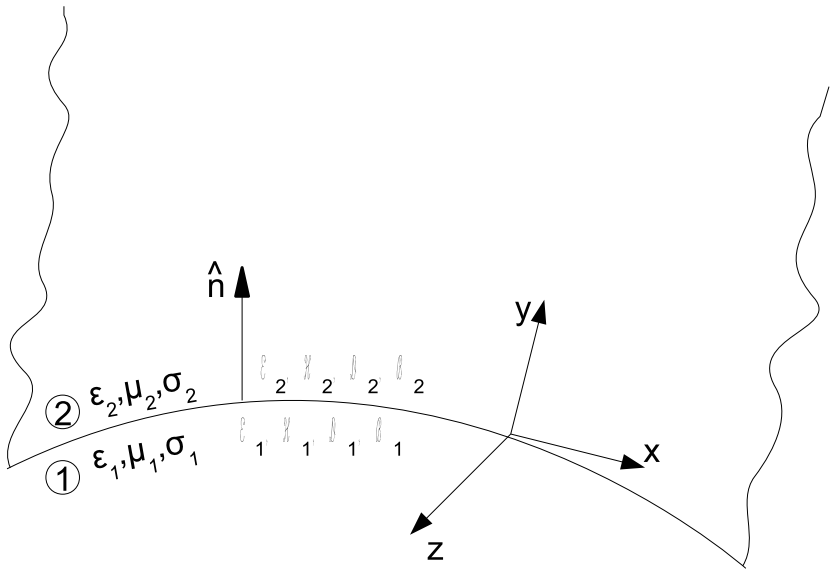

Figure 3.5: Boundary conditions between two media drawn in [1].

supported inside medium 1, therefore

$$\mathcal{E}_1 = 0. \tag{3.13}$$

And from Maxwell's equations, the tangential electric fields are continuous, where

$$\mathcal{E}_{1t} - \mathcal{E}_{2t} = 0 \Rightarrow \mathcal{E}_{1t} = \mathcal{E}_{2t}. \tag{3.14}$$

Then we find that

$$\hat{n} \times \mathcal{E}_2 = 0 \Rightarrow \mathcal{E}_{2t} = 0 \tag{3.15}$$

Basically, this tells us that, with respect to high electric fields, the most susceptible position within the element aperture when the incident wave is linearly polarized

will be in the center of the aperture width. This applied electric field will also be combined with the incident electric field that may be greater than the incident wave. In many applications for FSS, this increased total electric field at the plane of the element aperture is not a reason for concern. However, in HPM applications where the incident wave is already near the breakdown of air ($3MV/m$), the values of this total aperture electric field can be much more than the breakdown of air. Air breakdown, or any dielectric breakdown, occurs when the present electric field causes the surrounding media to ionize. When pushed above it's breakdown limit bound electrons will be released and convert the previously non-conductive material to conduct electricity in the form of an arc.

The easiest way to visualize this phenomenon is to observe a piece of somewhat crumpled aluminum foil in a microwave oven. Most people will know that when the microwave oven is started, the aluminum foil starts to spark. The electric field is increasing on the pointed corners and surfaces such that the air breaks down and arcs across toward surrounding aluminum to continue current flow.

The same happens with the FSS as the electric field approaches the boundary of the aperture and forms an electric field within the aperture. As seen in the CST MICROWAVE STUDIO® simulation snapshot in Figure 3.6, the darker colors show the concentrated electric field near the edge of the FSS apertures.

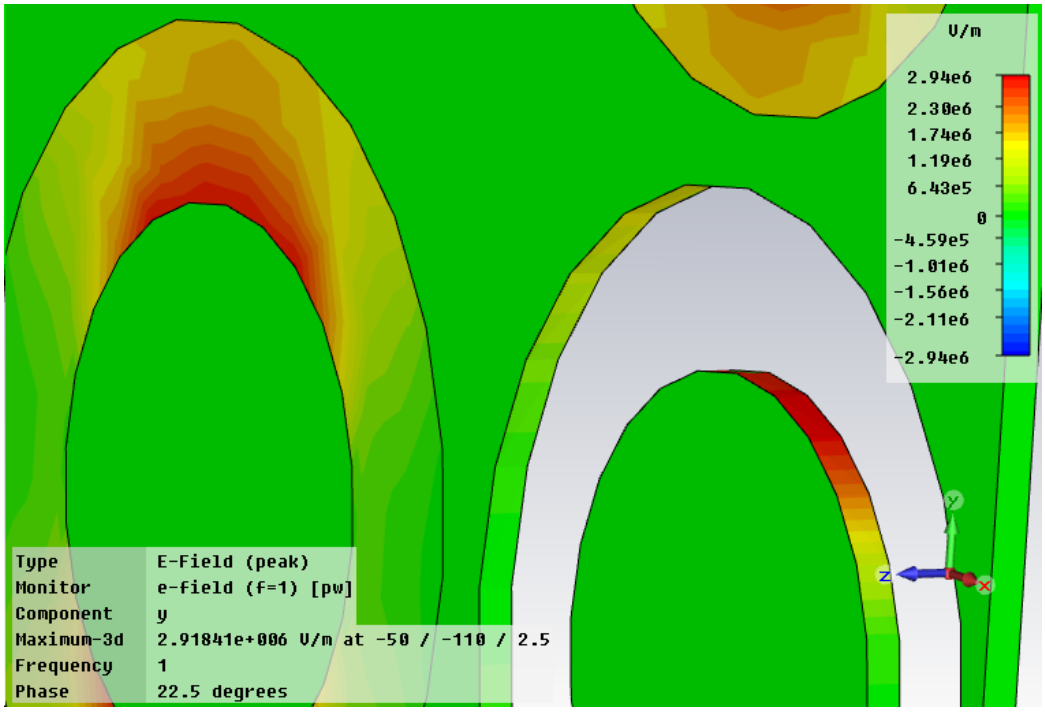

Figure 3.6: Peak electric field of a ring shaped element where the red colors indicate the higher electric field and the green is neutral. This example is using an incident wave with the electric field in the y-direction normal to the surface.

As can be seen by Figure 3.6, the predominant shape that was used is the ring shape. With its transmission qualities for the oblique incident waves, this shape will be best to investigate to see if it can withstand the high power fields.

3.5 Simulations

Using a good electromagnetic simulation is imperative to understanding the phenomenon of high power EM interaction with FSS. Since the option of fabricating a FSS sample and testing at power levels close to the breakdown limit of air could prove to be dangerous and detrimental to testing systems, a simulator based study is performed here.

CST MICROWAVE STUDIO® is and effective software package that is powerful and relatively easy to understand and implement. The basic package is a electromagnetic field simulation software that utilized several different solvers to achieve optimal results. The four solvers that are available to use consist of a transient solver, a frequency domain solver, an integral equation solver and an eigenmode solver.

The most flexible solver in the package is the transient solver, which was used in Figure 3.6. This solver allows one to get an entire broadband frequency behavior in a particular simulation instead of a frequency step approach, as in the frequency domain solver.

The next solver is the frequency domain solver which is best for electrically small structures. Although run time is longer, the frequency domain solver is better

when calculating S-parameters for strongly resonating structures. This method was used when evaluating different shapes for the FSS.

The third method is for electrically large structures, where it is noted that the volumetric discretization methods generally suffer from dispersion effects. Therefore, CST MICROWAVE STUDIO® includes an integral equation based solver that uses the multilevel fast multipole method (MLFMM). Even at lower frequencies where the MLFMM may not work as efficiently, an iterative method of moments solver is available.

The last solver is directed towards users evaluating filters. The eigenmode solver is used to determine the operating modes of the filter rather than a detailed study of the S-parameters.

Now that an overview of the simulation assumptions and settings have been given, the results of various FSS scenarios will be investigated for the purpose of determining optimal designs for mitigating breakdown.

IV. Results

In this chapter, the results of the FSS simulations are discussed and outlined.

4.1 FSS specifications

As noted in the previous chapter, a suitable shape for the individual elements were needed. To keep things from getting overly complicated, two different shapes were investigated, namely, the rectangle and ring shapes as shown in Figure 4.1. The corresponding CST MICROWAVE STUDIO® models of the rectangular slot and ring are shown in Figures 4.2 and 4.3.

Initially, a multiple aperture unit cell was investigated for the purpose of visualizing surface effects. However, modeling and run time became prohibitive. Thus, only one single aperture was modeled, being justified by the findings in [12]. Figure 4.2 is set up with the face of the FSS in the x-y plane and the "open" boundary is on the $\pm z$ axis. All of the simulations for this study were reproduced with these coordinate orientations. Also, note that the x-y-z directions of the model are shown in the lower right hand corner of the figure.

In regards to the ring element, as shown in Figure 4.3, the circumference is just under the free space wavelength λ_0 length of $300mm$. Also the distance between each corresponding ring is kept small at $140mm$ between the center of the ring to its closest neighbor in both the x and y directions. The thickness of the gap, however is a little bigger than what normally appears. This was done as a precaution of the

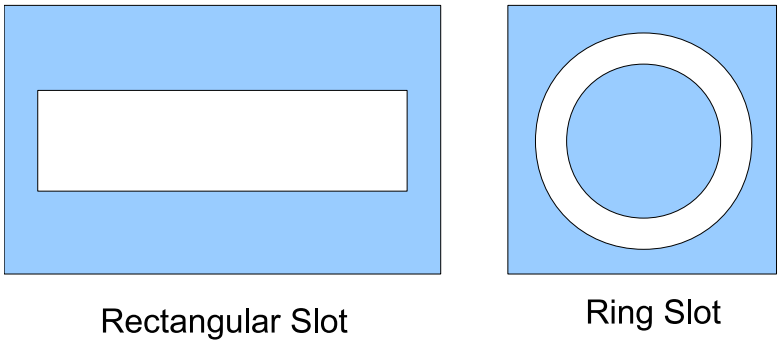

Figure 4.1: Basic rectangle and ring shaped elements that were investigated. The rectangle was a good choice because of its ease of interpretation and the ring shape because of the recommendation due to its effectiveness in handling oblique angles of incidence.

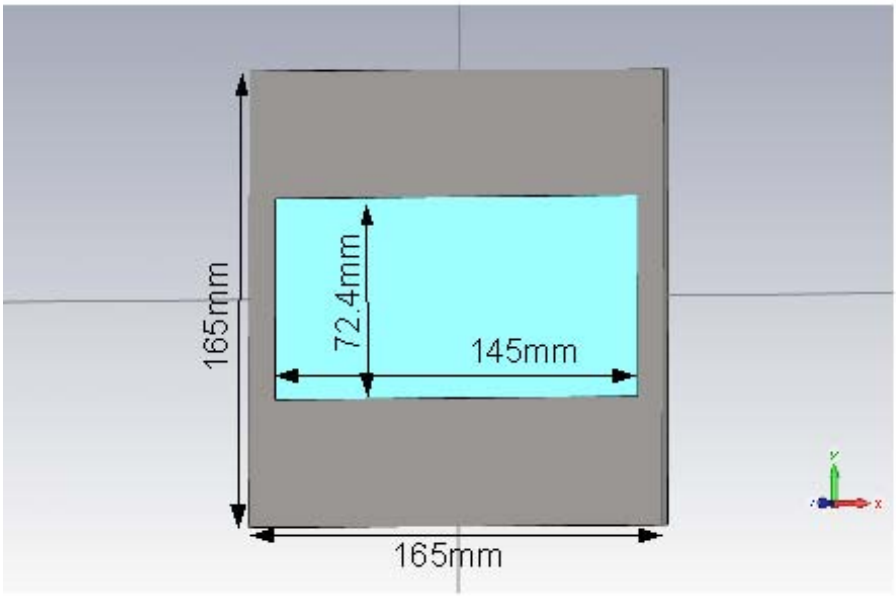

Figure 4.2: Rectangular unit cell rendered using CST MICROWAVE STUDIO® graphical user interface.

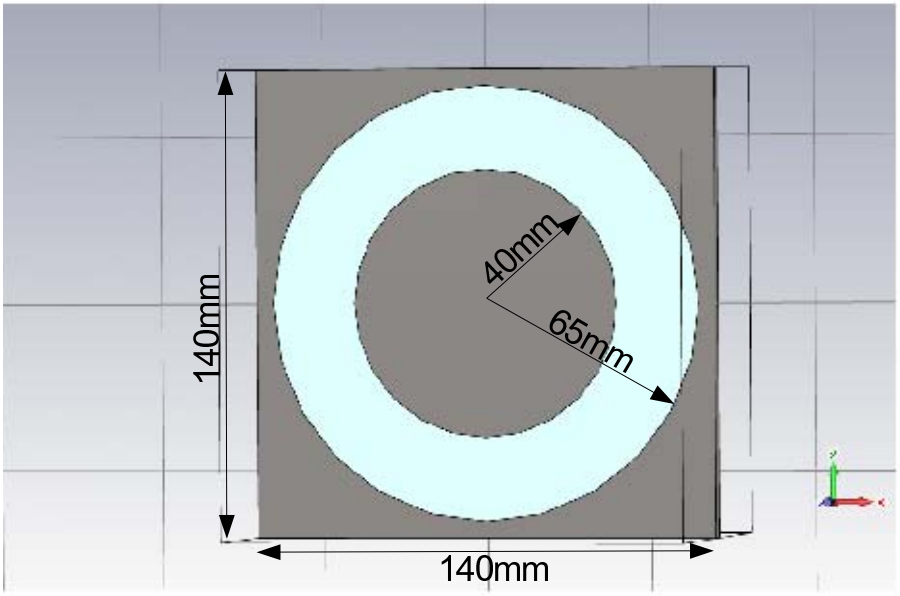

Figure 4.3: The ring unit cell rendered using CST MICROWAVE STUDIO®.

very high electric fields that are going to be introduced. If the gap is too narrow, the chance of breakdown will become greater as the electric field will be higher.

4.2 Dimensions to use for simulations

The dimensions used for the simulations were all based on wavelength of about $1GHz$. Contact at the Air Force Research Laboratory suggested that the desired operating frequency range would be L-band between $1-2GHz$ with a power density of about $0.5-1MW/cm^2$ with a $100ns$ pulse.

Using [6] as a reference that discusses the power handling of the FSS, he starts an example using an incident power density of $1MW/m^2$. Munk then calculates the incident electric field to be $E^i = \sqrt{10^6 \cdot 120\pi} = 1.94 \cdot 10^4 V/m$. This example provides

a measure of the power levels investigated, namely, $0.5 - 1MW/cm^2$. To equate them, one only has to convert the units from MW/cm^2 to its corresponding value of $1cdot10^4MW/m^2$. Therefore, the incident electric field for this power density is

$$E^i = \sqrt{10^{10} \cdot 120\pi} = 1.94 \cdot 10^6 V/m \text{ or } 1.94MV/m, \tag{4.1}$$

which is close to the breakdown of air at $3MV/m$. This is the very essence of the issue with such high powers. The FSS does not even have a bit of room to deal with. With that, a conservative field strength of $0.5MV/m$ was selected to avoid this breakdown limit.

The rectangular unit cell dimensions selected were $165mm$ square with the aperture size of $145mm \times 72.4mm$. The thickness of the slab is set at $5mm$. The ring unit cell dimensions selected were $140mm$ square with aperture outer radius of $65mm$ and an inner radius of $40mm$. The ring also has a $5mm$ thickness.

Note, when using the patch surface, one would evaluate the electric current induced on the metal patches. The current would resonate and then reflect at the desired frequency. More specifically, in the rectangular shape example, the incident electric field would need to be lined up with the $\lambda/2$ length side of the patch. However, when dealing with the aperture FSS, the electric field is not going to resonate in the aperture as an induced electric current. Instead, one needs to look at the induced magnetic current in the aperture, therefore lining up the incident magnetic current with the $\lambda/2$ length of the aperture.

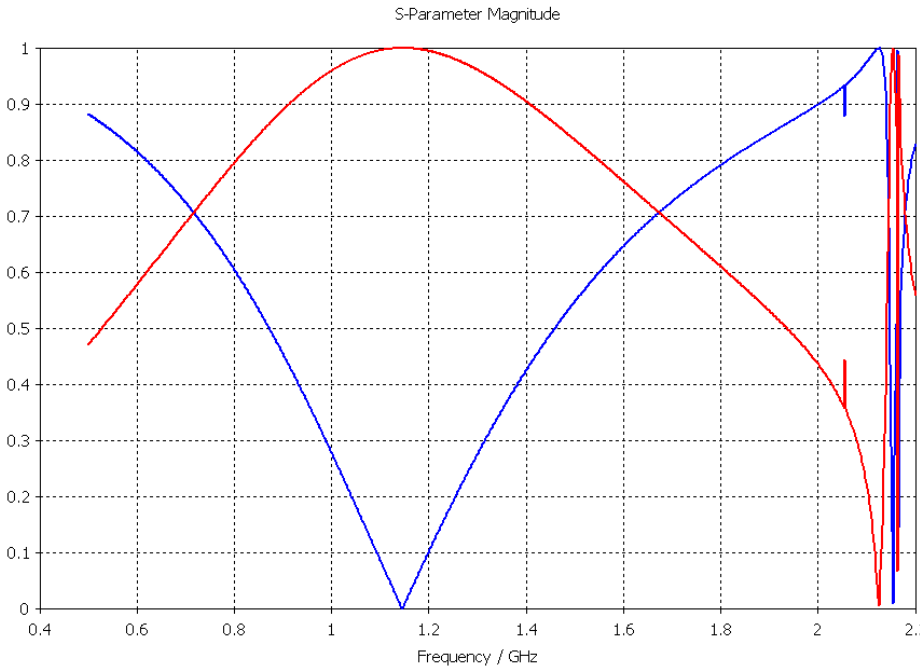

Figure 4.4: S-parameter graph example showing the transmission and reflection of incident waves at a range of frequencies.

4.3 S-parameters in the design

Getting the right size of the aperture is critical to making sure the pass-band is met. To figure out if the geometry would react to the incident wave, scattering parameters (S-parameters) were utilized. In CST MICROWAVE STUDIO®, the S-parameters were given when the frequency domain solver was being used.

In Figure 4.4, the S-parameters are graphed in the manner from which the ring shaped elements produced. As seen, the red line that peaks in the middle, is considered the S_{21} parameter in that it is represented by the magnitude of the transmitted wave over the magnitude of the incident wave. Likewise, the blue line that goes to zero in the middle of the graph is the S_{11} parameter, which is given by the magnitude of the reflected wave over the magnitude of the incident wave. Referring back to the two

port network example,

$$S_{11} = \frac{b_1}{a_1} \text{ and } S_{21} = \frac{b_2}{a_1}, \tag{4.2}$$

where a_1 is the incident wave magnitude and b_1 and b_2 are the reflected wave magnitude and transmitted wave magnitude, respectively. It is quite easy to interpret this graph when trying to see if the FSS is transmitting effectively, which is how the S-parameters were used in evaluating the size and shape of the individual elements. This is also where problems can be taken care of as was discussed before about the orientation of the incident wave compared with the elements. For example, in the rectangular shaped aperture, if the electric field of the incident wave is in line with the long end of the aperture, the S_{11} parameter will be very close to one for the same frequency sweep as seen in Figure 4.4. This is simply because the incident wave is reflected at lower frequencies due to the lack of resonance and low electric field in the aperture. And on the other side, the value of S_{21} will be near zero.

4.4 Incident wave

To evaluate the FSS in CST MICROWAVE STUDIO®, a few concessions have to be made and then the evaluation of possibilities have to be considered. First, when using periodic boundaries in the simulations, two of the three dimensions are set as the periodic boundaries, while the third dimension is considered to be open. The open boundaries imply that there will be not reflection from those directions. Thus, in the simulations, the incident wave was set to propagate from the $+z$ direction toward the $-z$ direction. This then sets the periodicity in the $x - y$ directions. The limitation

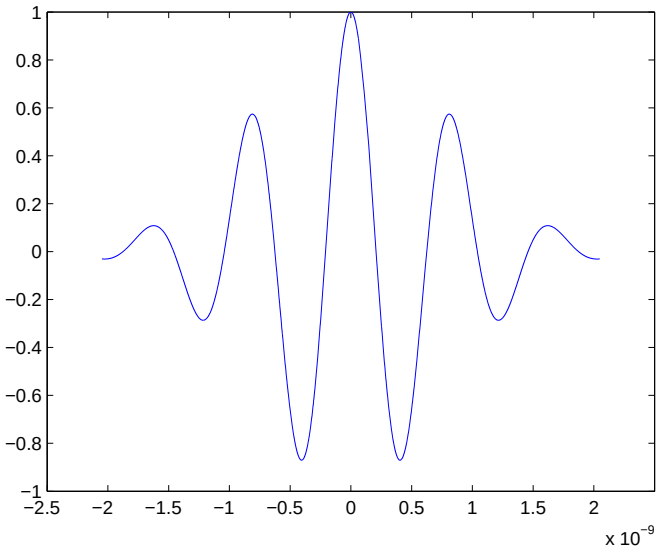

Figure 4.5: A Gaussian wave generated in Matlab® that is used to evaluate the frequency response of the FSS. The incident wave had a frequency span between $0.5 - 1.8GHz$. This gave the S-parameters that were used to determine the frequency where the transmission frequency would be.

is that these simulations cannot be run using an oblique angle, unless a finite sized surface is used. However, this introduces edge diffraction effects.

In regards to the incident wave, a Gaussian distributed wave that covers a range of frequencies was selected to investigate the frequency response of the FSS. An example of the Gaussian pulse that was used that provided a bandwidth to determine the response of the FSS is seen in Figure 4.5.

Then, setting up probes for the electric field and/or the magnetic field, one could see how the magnitude of the incident field was transmitting at the desired frequency, but reflecting the others. To get an idea of this phenomenon, Figure 4.6 may be addressed. In Figure 4.6 the golden colored curve is the incident wave. The incident wave is not the pure Gaussian wave, however, because of the reflected waves

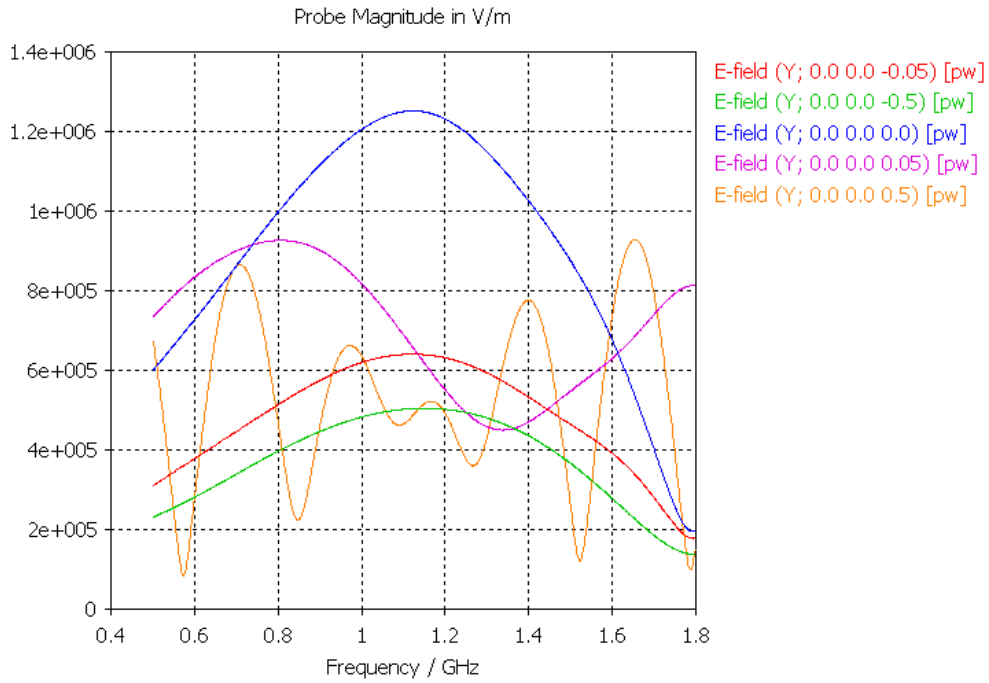

Figure 4.6: Scattered waves from Gaussian incident wave. The curves that only have one peak indicate the wave being transmitted at one frequency, while reflecting surrounding frequencies.

adding to its shape. The blue, red and green waves are probed at the center of the FSS ($z = 0$), and beyond. This one peak denotes that the center frequency is transmitted, while the frequencies around the center frequency are reflected by an increasing amount the further away from the center frequency.

While this Gaussian wave is good to determine the ability to reflect and transmit at a certain frequency, a stepped sine with a magnitude of $0.5MV/m$ and a frequency of $1.14GHz$ was employed to evaluate the electric fields in and around the FSS. With this type of incident signal, most of the signal should theoretically pass through the FSS. With $0.5MV/m$, as described before, the peak electric fields at the interface of the aperture could be realized.

4.5 Observing peak electric fields

4.5.1 Changing the incident field. The incident field was changed from the Gaussian wave to a sine step wave. The Gaussian wave produced the results as seen in Figure 4.6. This does show how the incident wave was transmitted and its magnitude was around $0.5MV/m$ at about $1.14GHz$, which was the overall magnitude of the incident wave. However, with a switch to the sine step incident wave, the responses changed a bit.

In the rectangular geometry, results as seen in Figure 4.7 indicate that the electric field did in fact transmit successfully. It did have some reflection as seen in Figure 4.7a, but that is offset by the reduction in the magnetic field as seen in Figure 4.8a. The difference in the electric field on the transmitted side of the FSS can just be detected by the graph in Figure 4.7d, as the amplitude is right near the $0.5MV/m$ level.

After obtaining the results with the rectangular shaped elements, the ring shaped elements were investigated using the frequency domain solver. Good transmission characteristics within the frequency range of $1-2GHz$ were achieved as shown in Figures 4.9 and 4.10.

4.5.2 Perfect electrical conductor and vacuum simulations. Working with the two geometries using Perfect Electrical Conductor PEC and vacuum media, the geometries are calculated based on free space wavelength parameters. Figures 4.9 and 4.10 were generated under these conditions.

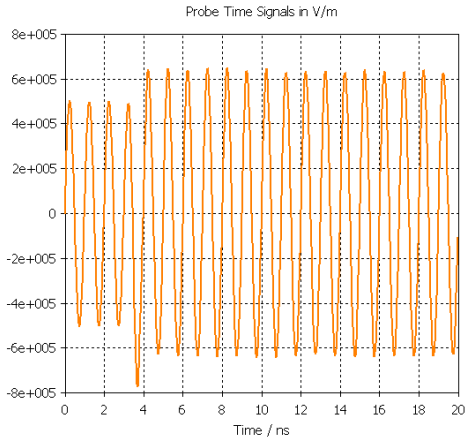

(a) E-field at $z = 0.5m$ on incident side of FSS.

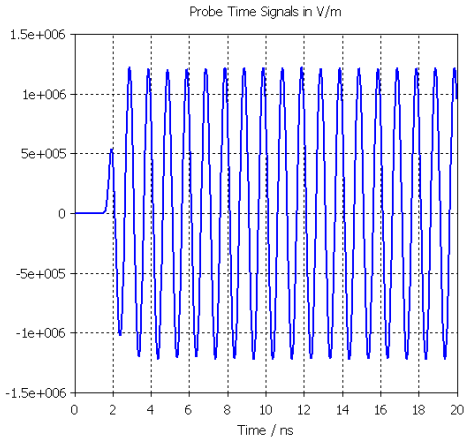

(b) E-field at $z = 0.0m$ inside the FSS aperture.

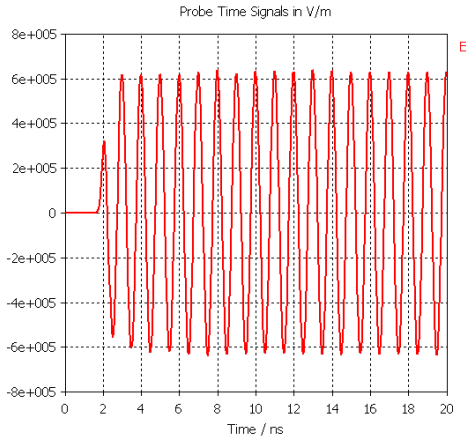

(c) E-field at $z = -0.05m$ on the transmitted of FSS.

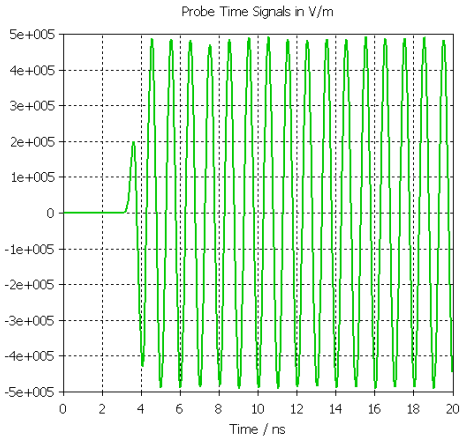

(d) E-field at $z = -0.5m$ on the transmitted of FSS.

Figure 4.7: Graphical comparison of the electric field with an incident sine step wave of $0.5MV/m$ at $1.14GHz$ that lasts for $20ns$. As can be seen, the electric field does transmit at the given frequency, however a reflection is noticed in the incident wave.

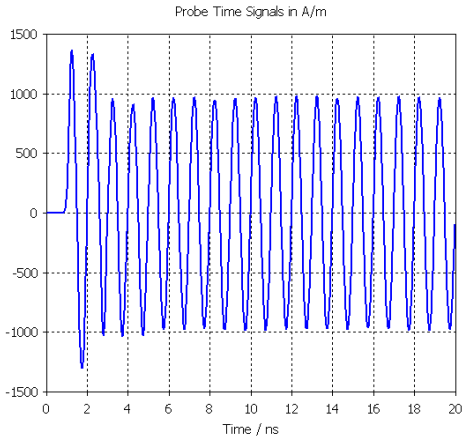

(a) H-field at $z = 0.2m$ on incident side of FSS.

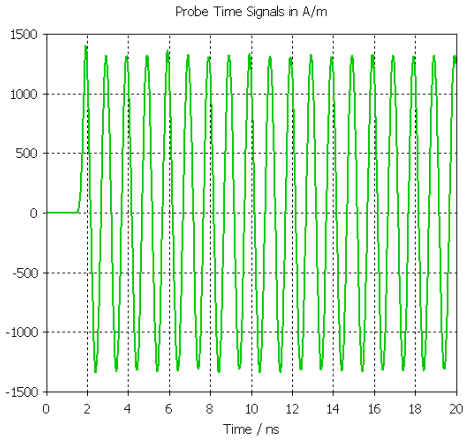

(b) H-field at $z = 0.0m$ inside the FSS aperture.

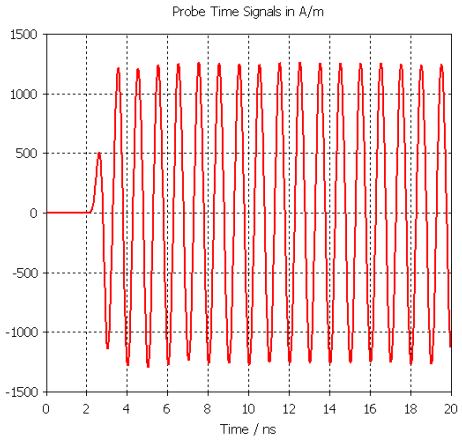

(c) H-field at $z = -0.2m$ on the transmitted of FSS.

Figure 4.8: Graphical comparison of the magnetic field with an incident sine step wave of $0.5MV/m$ at $1.14GHz$ that lasts for $20ns$. Here, the magnetic field decreases with the reflected wave, meaning that the reflected magnetic field was out of phase with the incident wave.

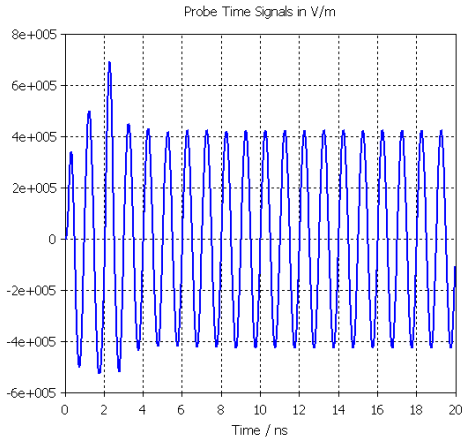

(a) E-field at $z = 250mm$ on incident side of FSS.

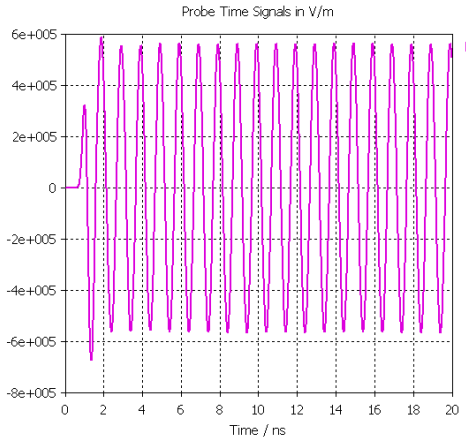

(b) E-field at $z = 50mm$ inside the FSS aperture.

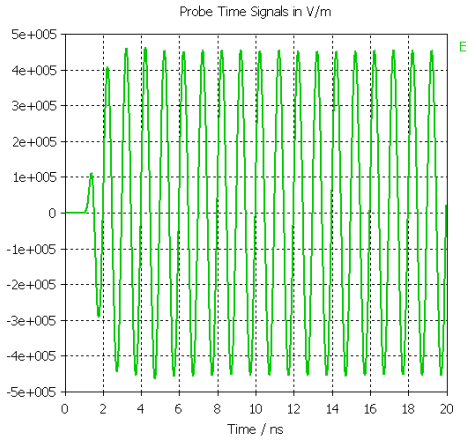

(c) E-field at $z = -50mm$ on the transmitted of FSS.

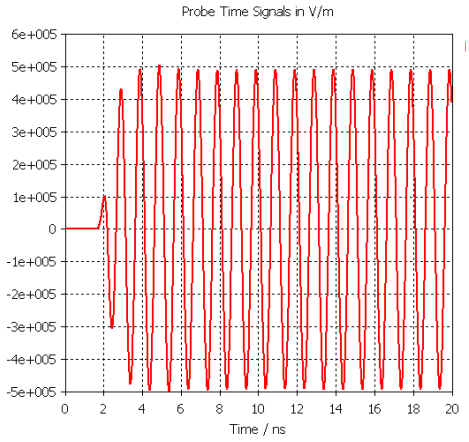

(d) E-field at $z = -250mm$ on the transmitted of FSS.

Figure 4.9: Graphical comparison of the electric field with an incident sine step wave of $0.5MV/m$ at $1GHz$ that lasts for $20ns$. As can be seen, the electric field does transmit at the given frequency, however a reflection is noticed in the incident wave.

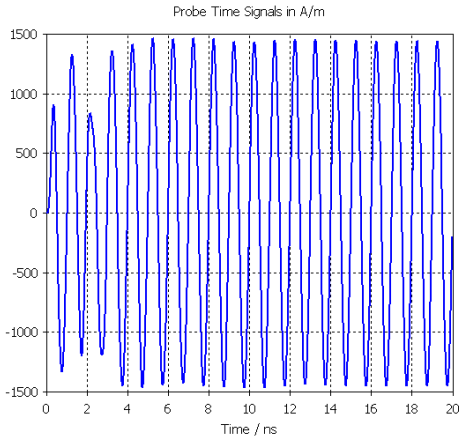

(a) H-field at $z = 250mm$ on incident side of FSS.

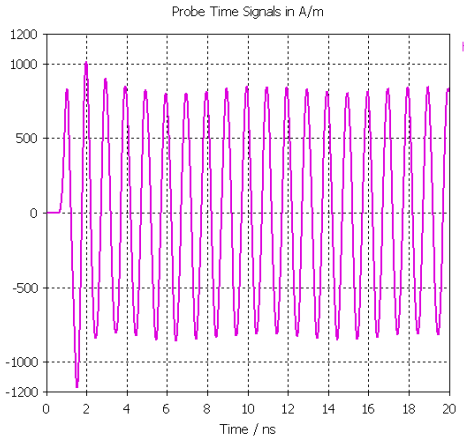

(b) H-field at $z = 50mm$ inside the FSS aperture.

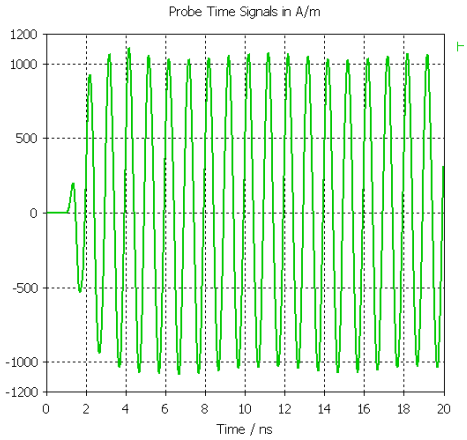

(c) H-field at $z = -50mm$ on the transmitted of FSS.

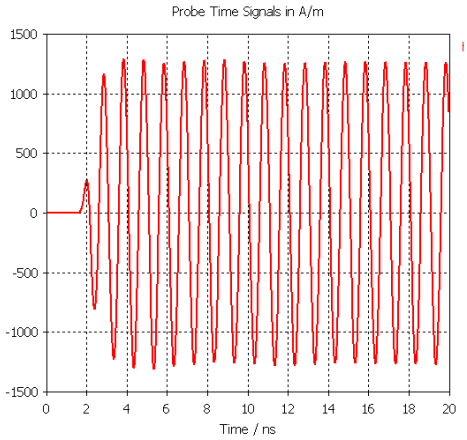

(d) H-field at $z = -250mm$ on the transmitted of FSS.

Figure 4.10: Graphical comparison of the magnetic field with an incident sine step wave of $0.5MV/m$ at $1GHz$ that lasts for $20ns$. As can be seen, the magnetic field does transmit at the given frequency, however a reflection is noticed in the incident wave variations.

As before, there is a reflection seen in the incident side signal. However, as seen before in the rectangle, the electric field is reduced in amplitude by about 18% and the magnetic field is increased, also by about 18%. This does not affect the transmitted wave significantly because the electric field is observed to have nearly $0.5MV/m$ amplitude. Also of note is the magnetic field that has about $1250A/m$ amplitude which is what it is before a portion of the reflected wave affect the incident wave. Although these values do not exactly match in amplitude, the total energy is transmitted. Examining the data, the results showed that the total energy on the transmitted side of the FSS was very close to the energy on the incident side, concluding that conservation of energy was preserved.

These peak electric fields are at the surface of the FSS. That is to say, they have to be dealt with on the plane of the FSS. As can be seen in the Figure 4.11, the red color indicates where the electric field is the strongest. For the ring, the peak electric field is right off the inner disk conductor and decreases outward from that point. Even though the values only display the x and y directed electric fields, one can estimate the maximum $3-D$ electric field to be above $4MV/m$ with the maximum x dimension amplitude of $2.25MV/m$ and the maximum y dimension amplitude of $3.43MV/m$. This is at least 30% above the air breakdown level of $3MV/m$.

Pursuing an idea presented to change the shape such that the edges would not be right angles, the model was updated to have a radius edge on the ring. The thinking is that the electric current induced on the metal will not have the abrupt cut-off seen in the right angle surface, thus reducing the extreme electric fields applied

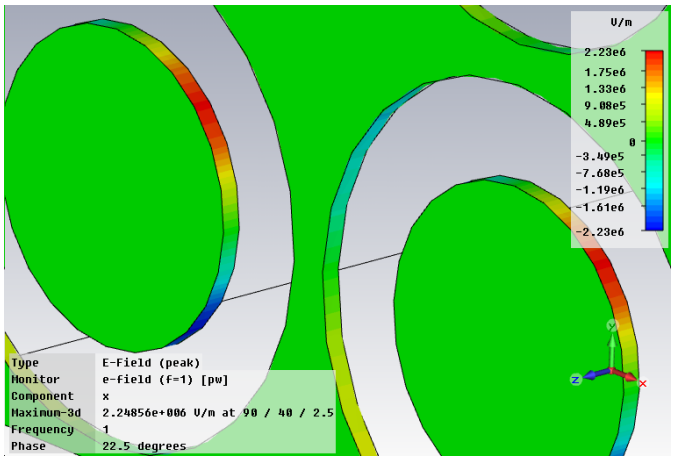

(a) $x - axis$ electric field distribution on ring element.

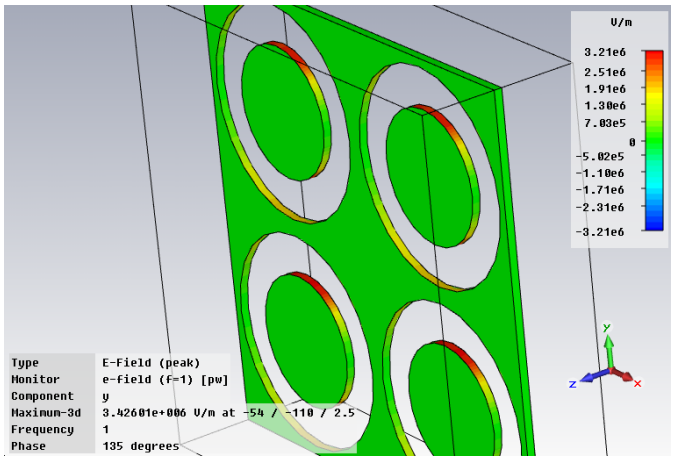

(b) $y - axis$ electric field distribution on ring element.

Figure 4.11: The electric field visual representation on the ring element. As can be seen, the peak electric field will be more than the breakdown of air ($3MV/m$).

across the gaps. This simulation was then performed with the results produced in Figures 4.12 and 4.13. Basically, the incident and transmission signals looked very close to the results in Figures 4.9 and 4.10. The noticeable difference showed up in the peak electric field Figure 4.14, where the decrease in surface thickness compresses the area for the electric field to be distributed. Therefore, the electric field increases quite a bit (more than $4MV/m$ in both the x and y directions). Therefore, no real benefit would be seen to use this method, especially since the point of this is to mitigate the higher electric fields.

4.5.3 Perfect electrical conductor and dielectric simulations. Using $0.5MV/m$ as the incident field has demonstrated that the peak electric fields at the interface of the FSS will be detrimental without some material in and around the FSS that can handle at least $7MV/m$. The best solution is to introduction dielectrics. The dielectrics can be used in the manner to hold the FSS pieces in place in the case of the rings and be an overall barrier for all applications. This will protect the metal from deterioration due to weather or other effects. Also, as noted in [6], dielectric breakdown levels do not vary due to air pressure differences. More specifically, air breakdown level varies as a function of air pressure, or altitude where other dielectric materials do not. This fact of the stability of dielectrics gives rise to use in airborne platforms. Airborne high power microwave systems may be a future study, given size requirements, but is still something to consider.

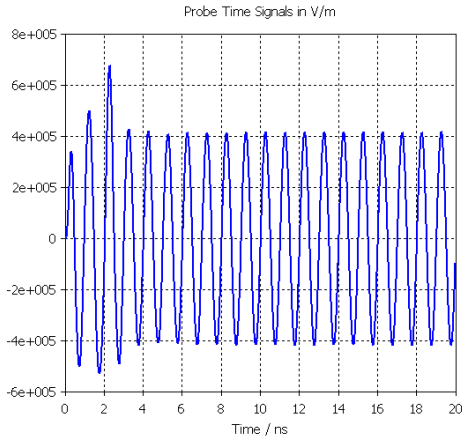

(a) E-field at $z = 250mm$ on incident side of FSS.

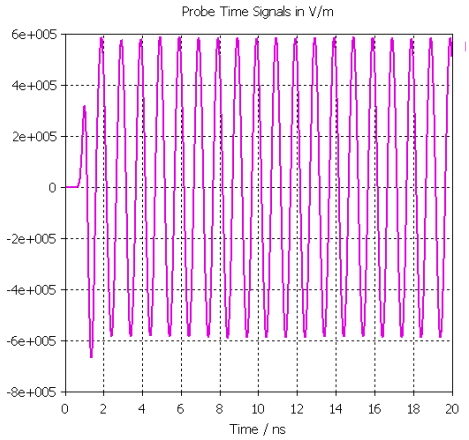

(b) E-field at $z = 50mm$ inside the FSS aperture.

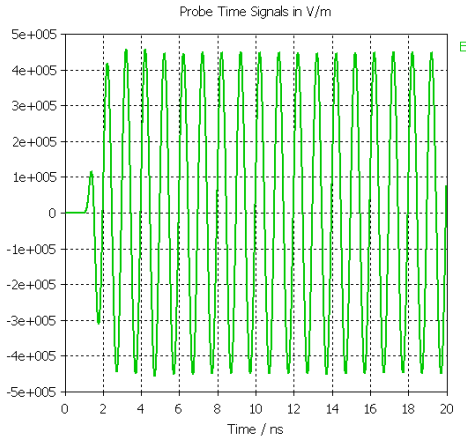

(c) E-field at $z = -50mm$ on the transmitted of FSS.

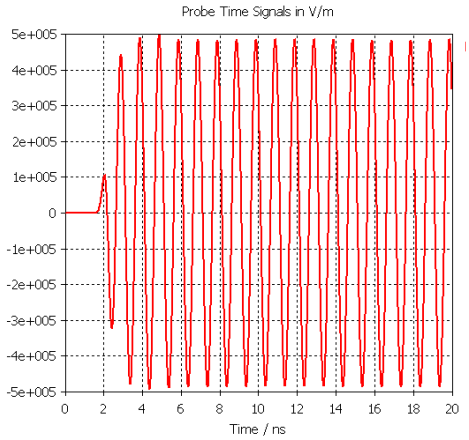

(d) E-field at $z = -250mm$ on the transmitted of FSS.

Figure 4.12: Graphical comparison of the electric field for the radius edged ring elements with an incident sine step wave of $0.5MV/m$ at $1GHz$ that lasts for $20ns$. As can be seen, the electric field does transmit at the given frequency, however a reflection is noticed in the incident wave.

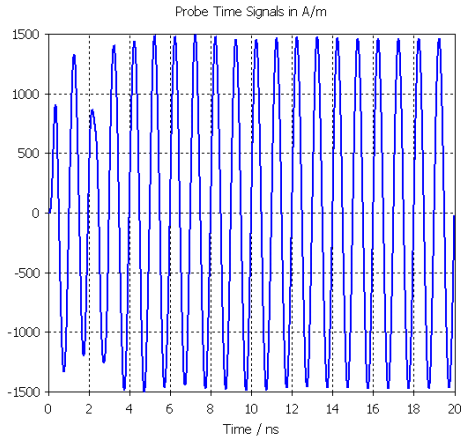

(a) H-field at $z = 250mm$ on incident side of FSS.

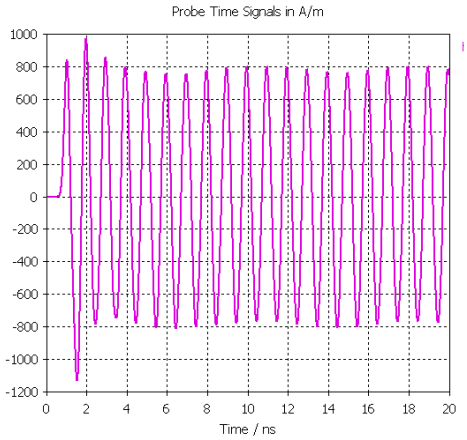

(b) H-field at $z = 50mm$ inside the FSS aperture.

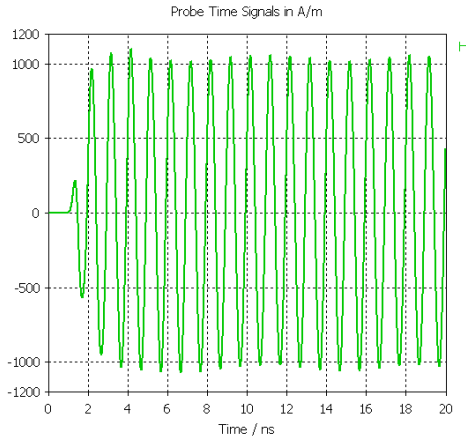

(c) H-field at $z = -50mm$ on the transmitted of FSS.

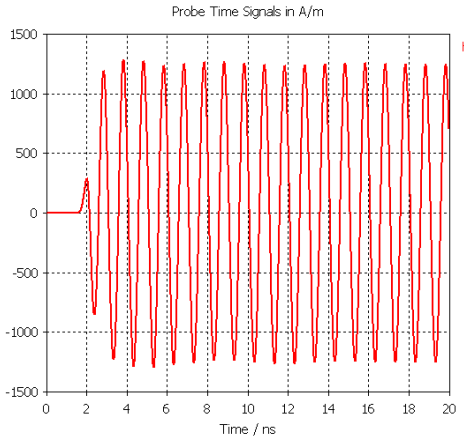

(d) H-field at $z = -250mm$ on the transmitted of FSS.

Figure 4.13: Graphical comparison of the magnetic field for radius edged ring elements with an incident sine step wave of $0.5MV/m$ at $1GHz$ that lasts for $20ns$. As can be seen, the magnetic field does transmit at the given frequency, however a reflection is noticed in the incident wave variations.

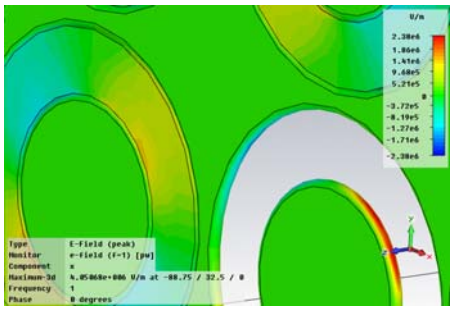

(a) $x - axis$ electric field distribution on radius edged ring element.

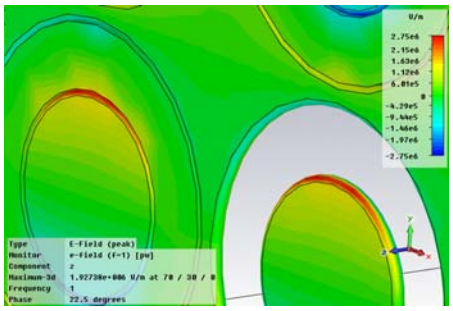

(b) $z - axis$ electric field distribution on radius edged ring element.

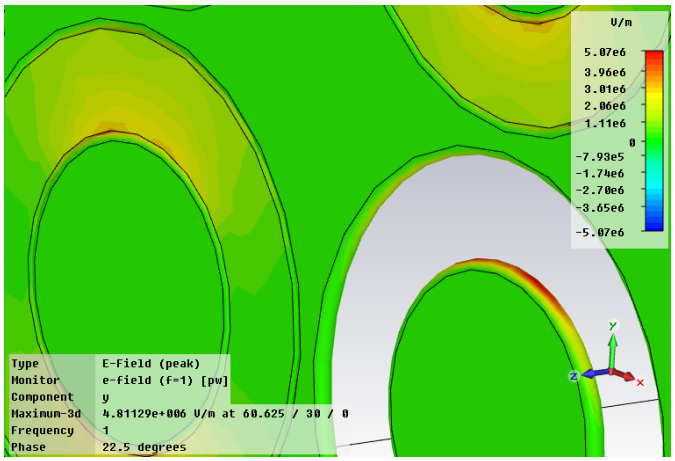

(c) $y - axis$ electric field distribution on ring element.

Figure 4.14: The electric field visual representation on the radius edged ring element. As can be seen, the peak electric field will again be more than the breakdown of air ($3MV/m$).

In [6], Munk explains reasons for including the dielectrics in the design of the FSS, since the dielectric material has considerable ability to aid in the shape of the transmitted wave. Among these abilities, the dielectric material helps to increase bandwidth, as well as stabilizes the pass band for different oblique incidence angles. Munk also describes the placement and thickness of the dielectric material to optimize efficiency. He states that the best placement is to enclose the FSS with equal thickness on both sides. More specifically, to get good signal transmission, Munk suggests $1/4\lambda_e$ thickness on each side of the FSS. Munk calculates this value of the effective wavelength (λ_e) by using Fresnel reflection coefficients. This will allow the signal to pass through the total material without much distortion. Part of the description of why the FSS needs to be embedded within the dielectric material is to mitigate the effects of the high electric fields at the surface of the FSS. He also suggests that a minuscule amount, on the order of $0.05\lambda_e$ of dielectric on each side of the FSS will suffice.

Consequently, dielectric materials with their properties available in CST MICROWAVE STUDIO® were added on both sides of FSS and within the apertures themselves. The thickness was varied to see the results on field strength on the transmission side of the FSS. The effective wavelength (λ_e) for $1GHz$ frequency in a dielectric called Arlon with $\epsilon_r = 3.25$ is $166mm$. Then $1/4\lambda_e$ would be $42mm$, which is relatively thick. Regardless, simulations were conducted to see the effect of increasing the thickness of the dielectric slabs. Figure 4.15 depicts the transmitted electric field strength compared to varying dielectric thickness. Arlon produces dielectrics for

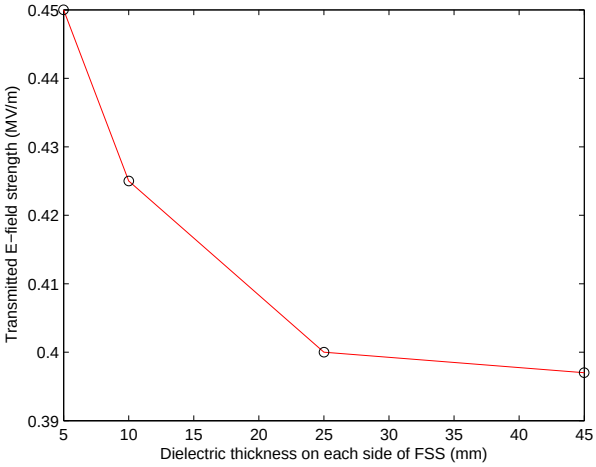

Figure 4.15: Graph comparing transmitted electric field strength compared to the thickness of the dielectric surrounding the FSS. As seen the field strength decreases rapidly as the thickness increases.

different applications including antennas. The graph does show that the transmitted electric field strength decreases by about 14% by the as the thickness approaches the $1/4\lambda_e$ thickness. The incident combined with the reflected wave was somewhat the same as the transmitted wave amplitude for the varying thicknesses.

As shown in Figure 4.16, the transmitted magnetic strength decreases on the same order as the electric field for the increasing thickness, but the total incident field increases.

4.5.4 Lossy metal and dielectric. Upon further examination, a lossy metal was used in conjunction with the dielectric. Silver was chosen for its low loss and high conductivity properties. Also, a dielectric with a lower dielectric constant was chosen (Arlon with $\epsilon_r = 2.5$). The results were somewhat predictable in that the signals transmitted sufficiently with a loss in the transmitted amplitude of about a

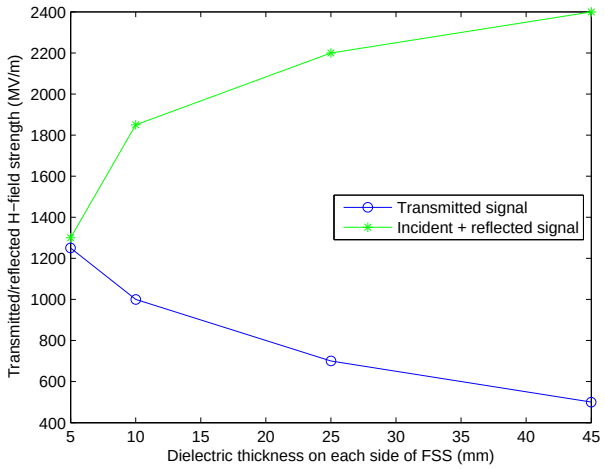

Figure 4.16: Graph of dielectric thickness versus the magnetic field strength on both the transmitted side and the incident side of the FSS.

10%. In Figure 4.17, the drop can be seen occuring after the signal reaches the FSS at about $2.5ns$. Also, the transmitted wave amplitude is just below the total incident wave at about $4.5MV/m$. The corresponding magnetic field in Figure 4.18 shows that a increase in the total incident magnitude to compensate for the decrease in the electrical field, but the transmitted magnetic field is less than the original incident field magnitude. This indicates that the energy transmitted is not concerved, which would be accounted for in the loss of the silver and dissipated as heat.

4.5.5 Maximum field strength versus distance from FSS. Next, the maximum field strength was observed to investigate at what distance the field strength reduces to the original levels, or at least to a level below the $3MV/m$ breakdown of air. The metal was chosen to be PEC of $0.5mm$ thick, while the dielectric was chosen to be made up of ideal 1.5 dielectric constant with a thickness of $2.5mm$ on either side of the FSS.

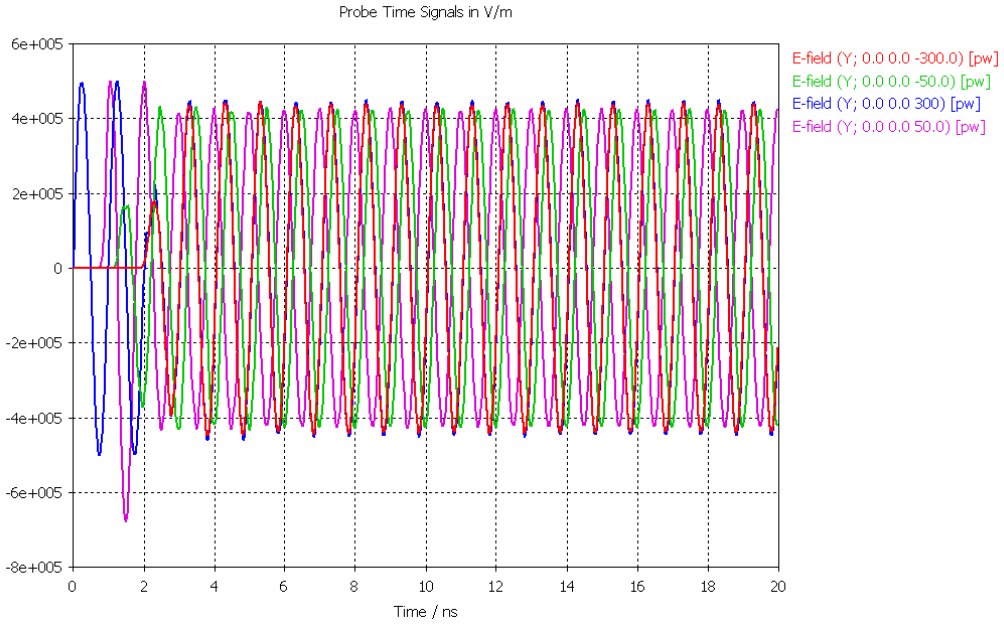

Figure 4.17: Electric field signals for silver/arlon FSS. The transmitted and incident/reflected waves both have slight reduction in field strength due to the loss component of the materials.

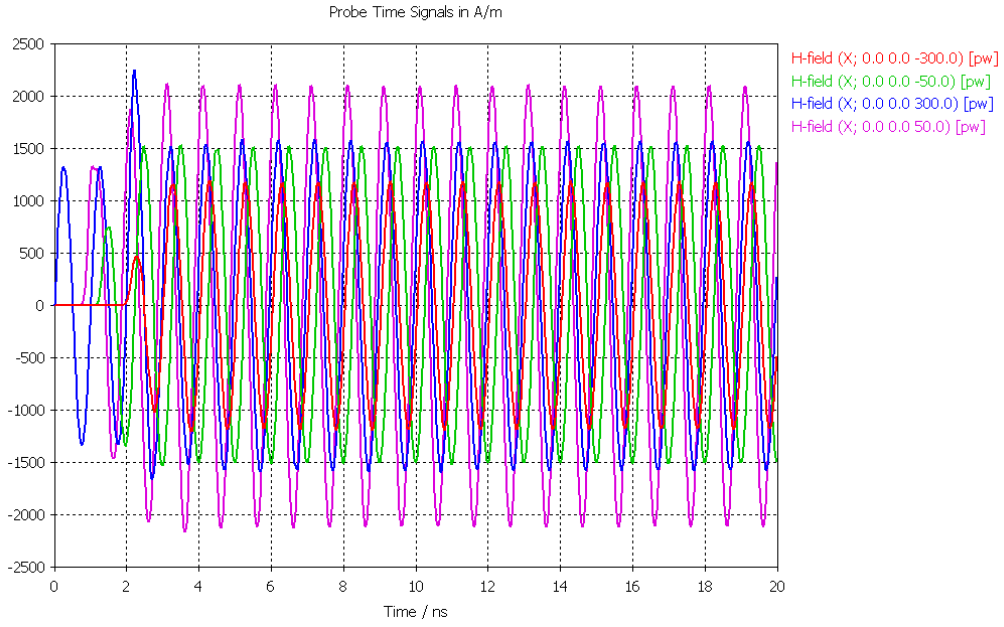

Figure 4.18: Magnetic field strength for silver/arlon FSS. As in the electric field before, the transmitted and the incident/reflected waves are both affected by the lossy material properties.

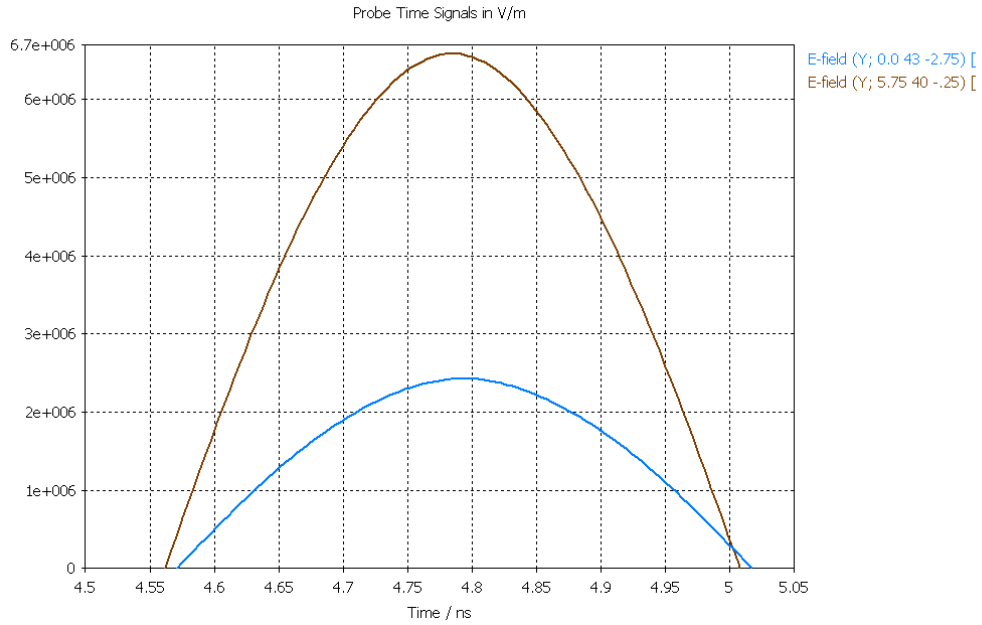

Figure 4.19: Maximum electric field in an ideal setup. The metal for the FSS is PEC, while the dielectric is thin with a dielectric constant of 1.5.

The motivation for this type of investigation was to see how far away from the interface of the aperture does the high electric fields extend. This would be critical in knowing how to make sure the dielectric is thick enough to prevent the air breakdown. As seen in Figure 4.19, the peak $\widehat{y}$-directed electric field is more than twice the breakdown of air ($3MV/m$). Without this dielectric, an arc would occur. The smaller curve on the figure is the peak level at the vaccuum/dielectric interface $2.5mm$ away from the metal. The difference is about a 64% drop in magnitude within that short distance. Now if the incident field level were to be more than $0.5MV/m$, the dielectric thickness would need to increase to accommadate.

The next plot in Figure 4.20 displays the mirror-like properties of the two sides of the FSS. the incident signal curve overlaps the transmitted signal curve, which again shows good transmission qualities.

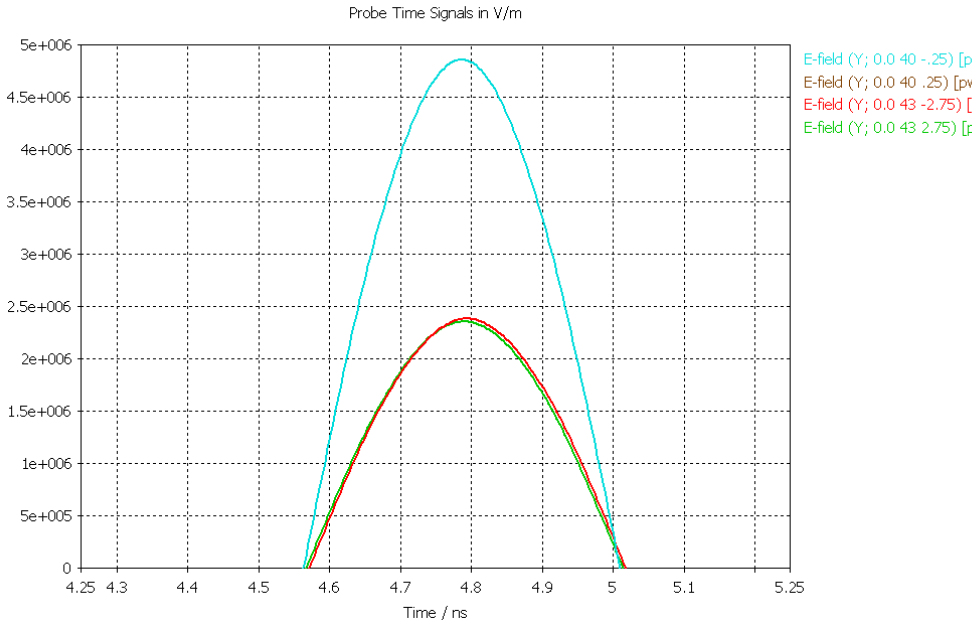

Figure 4.20: Mirror-like qualities of the signal through a PEC with good dielectric. The transmission signal pretty much overlays the incident signal.

Lastly, the surface area of the air/dielectric interface was scanned to observe the variation in the electric field and Figure 4.21 shows a couple of samples from that scan. Differing by only $2mm$ in the y direction, the amplitudes vary by as much as 9% in the positive y direction and almost 4% drop in the negative y direction. As expected, the magnitude continues to drop in all directions away from that position.

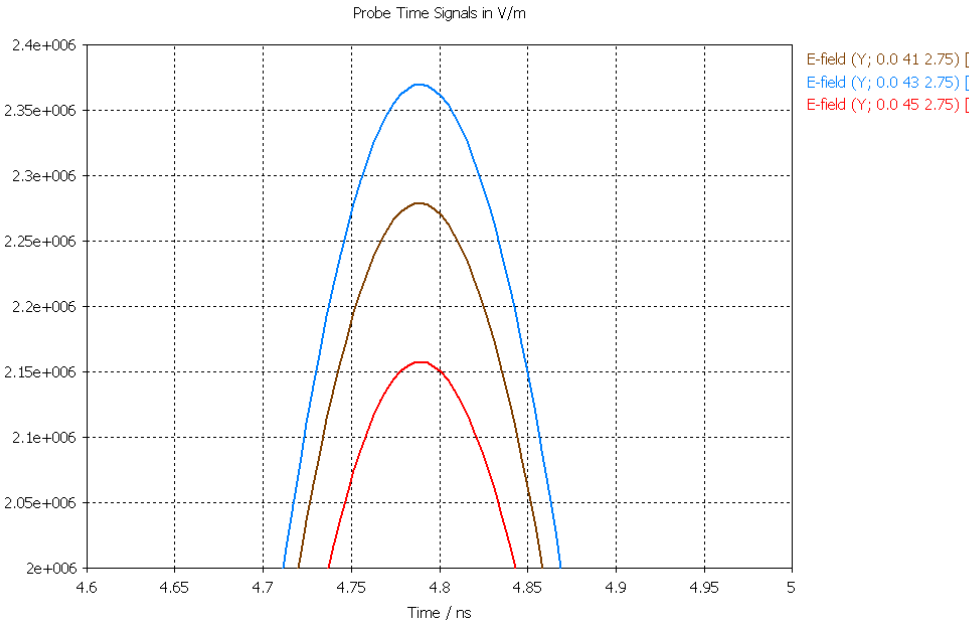

Figure 4.21: Variation of electric field probes in y direction at the air/dielectric interface

V. Concluding Evaluation and Further Study

Final thoughts about the research lend ideas that the use of Frequency Selective Surfaces (FSS) is not going to be totally forbidden. In fact, it may be quite a benefit in the future as High Power Microwave (HPM) systems become more mobile. The results do show that careful consideration of the applications and needs of the FSS will be imperative. That is to say that the particular application needs to warrant the use of FSS and one needs to be very careful on how to design the FSS to meet those needs.

5.1 Pick a shape

A large part of the design will come in the shaping of the FSS elements as was shown in this paper. The restrictions on the size of the elements will determine the pass band for the signal. As noted, some elements, such as loop elements, will transmit consistently at many angles of incidence. Then, there are just basic shapes, such as the dipole element that have limitations in that area but should not be disregarded. This does not even go into an unknown amount of more complex shapes that are probably only limited by manufacturing abilities.

Manufacturing the FSS will have to be considered, given the high power aspect. As the results showed, adding radius edges around the aperture will concentrate the high electric fields and create even more risk for breakdown. These may be altered by the tools used to etch the apertures out of the FSS.

Touching again on the size of the elements, one can imagine that if higher frequencies are used, then the element size decreases by an inversely proportional amount. This may both be a limiting factor on manufacturing and on breakdown limits of the materials.

5.2 Material selection

The materials will determine the quality of the transmitted wave. Given that the primary attention is to get as much energy to a target, all potential interference needs to be minimized. The loss in the materials can not be undone, but using highly conductive metals and low loss dielectrics is important. This will both reduce the deterioration of the signal, as well as reduce the heat generated by the loss in the materials.

Next, the materials need to be coherent with the way they react to one another. Harping back to design considerations, the materials selected need to be thoroughly tested to measure their respective thermal expansion. Ensuring their ability to expand and contract at the same rate will help reduce the risk of gaps or cracks forming and allowing for air breakdown to occur. This may even introduce a third material used to bond the metal and dielectric together.

5.3 FSS thickness

The thickness of the metal will need to be considered when determining the ability to withstand the amount of heat generated during the pulse. Systems today

may either be designed for continuous wave, single shot, or somewhere in between. This somewhere in between is basically a single shot that can be regenerated at a specified time interval (repetition rate). Once again each of these excel in certain applications. For instance, the continuous wave or high repetition rate system intends on heating up the target. Conversely, the single shot intends to get as much energy on the target to damage or at least alter the state of electronics. So, clearly a continuous wave with a higher average power might require a thicker plate to diffuse the heat, whereas the single shot, primarily consisting of high peak power, will require an adequately sized aperture to avoid breakdown and arcing.

Never forget the dielectric or leave as only a future add-on. As alluded to before, the dielectric is an integral part in the function of the FSS. It actually helps in many ways, including supporting the structure, frequency stability, and power handling of the FSS. The ring elements considered in this paper would not be able to stand alone without a dielectric of some kind to hold them in place. Many other shaped elements would require similar support. Also the frequency stability as the angle of incidence changes would be imperative for any non planar surface such as a radome that have curved shapes. And, as seen in this high power application, the FSS would almost certainly fail without the addition of dielectric materials to allow the presence of the high electric fields.

5.4 In closing

To wrap up this paper is just a way to say that a large area of research still needs to be performed. From materials to manufacturing, many areas are open to explore. The hope is that some of this effort may be applied in the future role of non-lethal weaponry.

Bibliography

1. Balanis, Constantine A. *Advanced Engineering Electromagnetics*. John Wiley and Sons, Inc., 1989.

2. Barker, Robert J. and Edl Schamiloglu. *High-Power Microwave Sources and Technologies*. IEEE Press, 2001.

3. Chen, Jacqueline C. and Phil H. Stanton. "Theoretical and Experimental Results for a Thick Skew-Grid FSS with Rectangular Apertures at Oblique Incidence". *IEEE Explore*, 1991.

4. English, Errol K. *High Power Multi-Layer Frequency Selective Surfaces*. Technical report, Mission Research Corporation, 1997.

5. Giri, D. V. *High-Power Electromagnetic Radiators, Nonlethal Weapons and Other Applications*. Harvard University Press, 2004.

6. Munk, Ben A. *Frequency Selective Surfaces Theory and Design*. John Wiley and Sons, Inc., 2000.

7. Parker, E. A. and S. M. A. Hamdy. "Rings as Elements For Frequency Selective Surfaces". *Electronics Letters*, 1981.

8. Rakowska, A. and K. Hajdrowski. "Influence of High-Voltage Polarisation on Impulse Breakdown of Polyethylene and Crosslinked Polyethylene". *IEEE 5th International Conference on Conduction and Breakdown in Solid Dielectrics*, 1995.

9. Sekil, Y. "A Consideration of the Breakdown Field Strength of XLPE Cable Insulation". *IEEE 5th International Conference on Conduction and Breakdown in Solid Dielectrics*, 1995.

10. Sipus, Zvonimir, Marko Bosiljevac, and Juraj Bartolic. "Rigorous and Approximate Analysis of Curved Frequency Selective Surfaces". *IEEE Explore*, 2008.

11. Wu, T. K. *Frequency Selective Surface and Grid Array*. John Wiley and Sons, Inc., 1995.

12. Zhang, Chenggang, Qiang Zhang, and MingChun Hu. "Adaptive Frequency Selective Surface with ring slot units". *IEEE Xplore*, 2007.

REPORT DOCUMENTATION PAGE

Form Approved
OMB No. 074-0188

1. REPORT DATE *(DD-MM-YYYY)*	**2. REPORT TYPE**	**3. DATES COVERED** *(From – To)*
25-03-2010	Master's Thesis	Sep 2008-Mar 2010

4. TITLE AND SUBTITLE

Investigating the Use of Frequency Selective Surfaces in High Power Microwave Applications

5a. CONTRACT NUMBER

5b. GRANT NUMBER

5c. PROGRAM ELEMENT NUMBER

6. AUTHOR(S)

Steven Pugh, Captain, USAF

5d. PROJECT NUMBER

5e. TASK NUMBER

5f. WORK UNIT NUMBER

7. PERFORMING ORGANIZATION NAMES(S) AND ADDRESS(S)
Air Force Institute of technology
Graduate School of engineering and Management
2950 Hobson Way
WPAFB OH 45433-7765

8. PERFORMING ORGANIZATION REPORT NUMBER

AFIT/GE/ENG/10-25

9. SPONSORING/MONITORING AGENCY NAME(S) AND ADDRESS(ES)

Intentionally left blank

10. SPONSOR/MONITOR'S ACRONYM(S)

11. SPONSOR/MONITOR'S REPORT NUMBER(S)

12. DISTRIBUTION/AVAILABILITY STATEMENT

Approval for public release; distribution is unlimited

13. SUPPLEMENTARY NOTES

14. ABSTRACT

This thesis explores new territory with the theoretical investigation of the use of FSS in HPM applications. Work was performed in a simulation environment where rectangular and ring-shaped FSS elements were evaluated. Incident electric field levels of 0.5MV/m were propagated toward the FSS in a plane wave that was perpendicular to the surface. Results show that the total electric field in the apertures of the FSS can reach more than 6MV/m. This necessitates the use of high strength dielectric materials surrounding the FSS to reduce the risk of electrical breakdown. It is shown that a dielectric of only 2.5mm thick on each side of the FSS eliminates the risk of breakdown.

15. SUBJECT TERMS

Frequency selective surfaces, periodic surfaces, high power microwaves, non-lethal weapons

16. SECURITY CLASSIFICATION OF:			**17. LIMITATION OF ABSTRACT**	**18. NUMBER OF PAGES**	**19a. NAME OF RESPONSIBLE PERSON**
REPORT	**ABSTRACT**	**c. THIS PAGE**			Dr. Michael J. Havrilla, michael.havrilla@afit.edu
U	U	U	UU	77	**19b. TELEPHONE NUMBER** *(Include area code)* (937)-255-6565, ext. 4582

Standard Form 298 (Rev: 8-98)
Prescribed by ANSI Std. Z39-18